A Multiphysics Study of Interfacial Properties of 3D Printed Filaments

By

Alireza Rezaee

Presented to the Faculty of the Graduate School of

The University of Texas at Arlington in Partial Fulfillment

of the Requirements for the Degree of

DOCTOR OF PHILOSOPHY

THE UNIVERSITY OF TEXAS AT ARLINGTON

Department of Mechanical and Aerospace Engineering

Acknowledgements

Undertaking this PhD wouldn't have been possible without the financial help, emotional support and technical guidance of many people.

First, I would like to express my sincere appreciation to DR. Ashfaq Adnan, for his encouragements and instructions. This work wouldn't have been completed without our after-hours meetings.

I would like to acknowledge the financial support from Triumph Aerostructures and Bell. Working at Bell and being part of this great company has been a true blessing.

I would also like to thank my dissertation committee for their insight and support throughout this research.

I am eternally grateful to my wife, Sadaf Y. Rezaee, for her unconditional love and support. Thank you for taking care of every chore in the house so I could study, and for sacrifices you made to help me make this work possible.

Dedication:

To the strongest woman I know, Sadaf Y. Rezaee.

Abstract:

Fused Deposition Modeling has become the most popular 3-D printing method over the last decade. Due to its potential to save time, cost and, labor, there is a great deal of interest to use this technique for production of functional load carrying parts and assemblies in bio-medical, automotive, aerospace, and oil and gas industries.

In general, materials used in FDM process are isotropic; however, parts printed using FDM process show anisotropic mechanical properties with inconsistent properties in the transverse direction to the filaments' cross-section. This anisotropic behavior is due to the fabrication process, and the inconsistency in the transverse mechanical properties are due to the different processing parameters used in the FDM process.

Transverse mechanical properties of FDM parts are developed as the extruded filaments come in contact and partially bond together. The quality of the bond at the interface of the filaments is the most important factor in the development of mechanical properties in the transverse direction.

Transient heat transfer, Multiphase fluid flow, molecular diffusion and structural fracture mechanics should be considered to study the development of interfacial mechanical properties between extruded filaments in FDM parts.

In this research, Multiphysics Numerical Modeling techniques have been utilized to study and understand the development of interfacial mechanical properties between adjacent filaments. Effect and significance of different parameters used in FDM process are discussed and suggestions are provided for improvement of the transverse mechanical properties of FDM parts. A new diffusion coefficient is also suggested for determination of interfacial material properties of FDM printed filaments.

Table of Contents

CHAPTER 1

CHAPTER 2

Nomenclature:

Unozz = Print Speed (Nozzle Speed)

Tamb = Ambient Temperature

Tnozz = Extruder Temperature

Tbed = Temperature of Bed

Cp = Specific Heat

K = Thermal Conductivity

ρ = Density

L = Length of Filament

d_f = Diameter of Filament

r = Radius of Filament

t = Time

I.I.L= Initial Interface Length

F.I.L = Final Interface Length

Tg = Glass Transition Temperature

Rho = Density

gp = Negative Gap Setting

TR(s) = Reptation Time

$\overline{N_{UD}}$ = Average free convection heat transfer coefficient.

R_{a_D}= Rayleigh dimensionless numbers

Pr = Prandtl dimensionless numbers

g = Acceleration of gravity

$\propto_p$ = Air's coefficient of thermal expansion

T_{ext} = Envelope temperature

h = Convective heat transfer coefficient

S = strain-rate tensor

f_{st} = Force per unit area due to the surface tension.

τ_i =Total stress tensor in the domain.

$\boldsymbol{u}_{mesh}$ = Velocity of the mesh at the interface.

n_i = Normal of interface.

∇_s = Surface gradient operator.

σ = Surface tension at the interface.

$\nabla_s . n_i$ = Mean curvature of the surface

gp = negative gap percentage

w = Strain energy density

J = J integral

SIF = Stress Intensity Factor

NSIF= Notch Stress Intensity Factor

J = J integral

SIF = Stress Intensity Factor

NSIF= Notch Stress Intensity Factor

KI_1 = Stress intensity factor (Mode 1)

J_1 = J-integral (Mode 1)

T = Traction Vector

tw = Diffusion Time

ω = Transformed variable in the frequency domain

P = Fourier transformation of the probability density function

δ= Dirac delta function

K = Fracture toughness

K_∞ = Fracture toughness of the fully healed filaments

σ = Ultimate strength

σ_∞ = Ultimate strength of the fully healed filaments

L_W = Minor chain length

Ft = Tangential force per unit area

ν = Poisson's ratio

E = Modulus of Elasticity

Chapter 1:

Introduction

1.1 Rationale for Proposed Research:

Fused Deposition Modeling has become the most popular 3-D printing method over the last decade. Due to its potential to save time, cost and, labor, there is a great deal of interest to use this technique for production of functional load carrying parts and assemblies in bio-medical, automotive, aerospace, and oil and gas industries. However, little is known about the important factors affecting the interfacial properties of the FDM filaments. Transverse strength of the FDM printed filaments is significantly lower than their longitudinal strength. This weakness in the transverse direction properties results in a general weakness of the FDM parts.

Due to the multi-physics nature of the process and the number of variables involved in the process there needs to be a comprehensive study of variables affecting the development of interfacial mechanical properties of the FDM parts.

1.2 Current State-of-the-Art:

Li and his colleagues [2] developed a one-dimensional transient heat transfer model with the assumption of uniform temperature distribution throughout the cross-section. In Li's model, conduction heat transfer with the foundation was considered in the form of convection and no phase change was considered in the analysis (consistent thermal properties). One dimensional models fail to predict the lateral thermal interaction of filaments. The complex boundary condition of the filaments also cannot be modeled with 1D modeling.

Rodríguez and his colleague[3] used a 2D analytical model to solve average temperature and assumed consistent thermal properties and boundary conditions for the filaments. Rodriguez

model has elliptical filaments with fixed boundary conditions. The model does not account for the change in the thermal properties and the boundary conditions of the filament.

Q.sun [4]and his colleague used the newtonian sintering model proposed by Pokluda [5] to predict the neck growth between the filaments. The proposed model for polymer sintering was not in good agreement with experimental results [6, 7]

Q.sun [4]concluded that the heat transfer models available in the literature are not adequate as they ignore the heat transfer through conduction within filaments and the change in the boundary conditions of the filaments during the FDM process.

For molecular diffusion modeling, there has been little to no research in literature. Q.sun in his research suggested an Arrhenius equation for molecular diffusion that this author believes the proposed equation doesn't satisfy the molecular diffusion requirement as the outputs of the equation do not fall under the acceptable diffusion range.

1.3 Scope of this research:

Fused deposition process is a highly nonlinear process with material and geometric nonlinearities. A detailed model of this process should include Thermal and Fluid analysis.

There is little to no numerical research available in the literature to study the effect of different parameters on the development of interfacial mechanical properties between extruded filaments. Most research published in the literature have used the isothermal Newtonian sintering model proposed by Pokluda[5] to estimate the degree of healing between the filaments and disregard the effect of molecular diffusion and fracture mechanics in the final mechanical properties of the FDM parts.

In general, the Newtonian sintering models available in literature are limited to constant temperature, viscosity and surface tension; however, these parameters are not constant in the FDM process.

It was determined that a series of Multiphysics numerical simulations of the FDM process covering the changes in heat capacity, boundary conditions, material properties of filaments including the non-isothermal viscous sintering and non-isothermal molecular diffusion are needed to understand this complex process.

This research includes 4 parts. The first part is a series of high fidelity transient thermal analyses of the FDM process. These models are used to study the effect of different variables in the thermal profile of filaments and temperature history of their interface during the FDM process.

The second part of this research is a series of non-isothermal multiphase flow simulations of FDM process to study the significance of the sintering process and neck's growth rate between the filaments.

The third part of this research is a series of non-isothermal molecular diffusion analyses of the FDM process to study the effect of different parameters in development of interfacial mechanical properties between extruded filaments.

The forth part of this research is a fracture mechanics study of the notch singularity existing at the interface of the filaments and effects of negative gap setting in the notch stress intensity factor of the FDM parts.

The goal of this research is to propose possible solutions to improve interfacial mechanical properties of FDM parts.

1.4 Background:

1.5 Three-Dimensional Printing Technologies:

The concept of 3-Dimensional printing was first introduced by Charles W. Hull [8] in 1986, in a US patent. 3-D printing is a technology that creates 3-Dimensional objects by adding materials layer by layer. with the advancements in computer processing powers, computer-aided design tools and computer tomography scans (CT) this method became more popular to researchers. Different methods have been utilized to add materials layer by layer. Per ASTM F2792, Fused deposition modeling (FDM)[9], stereolithography apparatus (SLA)[10], digital light processing (DLP)[11], and continuous liquid interface production (CLIP) [12] are some of the techniques used for the 3D printing process. Advancements in the fused deposition modeling along with the benefits of this technique have made it the most favorable method of 3D printing. These benefits include rapid production, low cost, ability to produce complex structures, ability to manufacture locally controlled properties[13], being environmentally friendly, and reducing the fastening process. Contrary to the traditional machining process, where the material is removed from a block, in the FDM process material is added layer by layer to create a 3D object.

Advancements in the fused deposition modeling along with the benefits of this technique have made it the most favorable method of 3D printing. These benefits include rapid production, low cost, ability to produce complex structures, ability to manufacture locally controlled properties [14], being environmentally friendly, and reducing the fastening processes. Contrary to the traditional machining process, where the material is removed from a block, in the FDM process material is added layer by layer to manufacture the part. Fused deposition modeling (FDM) was developed by Stratasys Inc.

The FDM machine is a Computer Numerically Controlled (CNC) machine with an extruder and a heating chamber. It uses extrusion method to add thermoplastic materials such as ABS, layer by layer. FDM was first patented in the US by Scott Crump in 1992.

Filaments made from different types of polymers, such as Acrylonitrile butadiene styrene (ABS), Polylactic acid (PLA), Polyethylene (PET), Polypropylene (PP) and Ultem 9085, are passed through a heating chamber and heated above the glass transition temperature. These monofilaments are then forced through the printer nozzle and deposited on a platform side by side. As the filaments lose heat, they bond together, change phase, and solidify.

FDM printed parts have lower fracture properties than injection molded parts as the adjacent filaments are not well bonded. The quality of the bond between extruded polymeric filaments is the most important parameter in the interfacial mechanical properties of FDM objects.

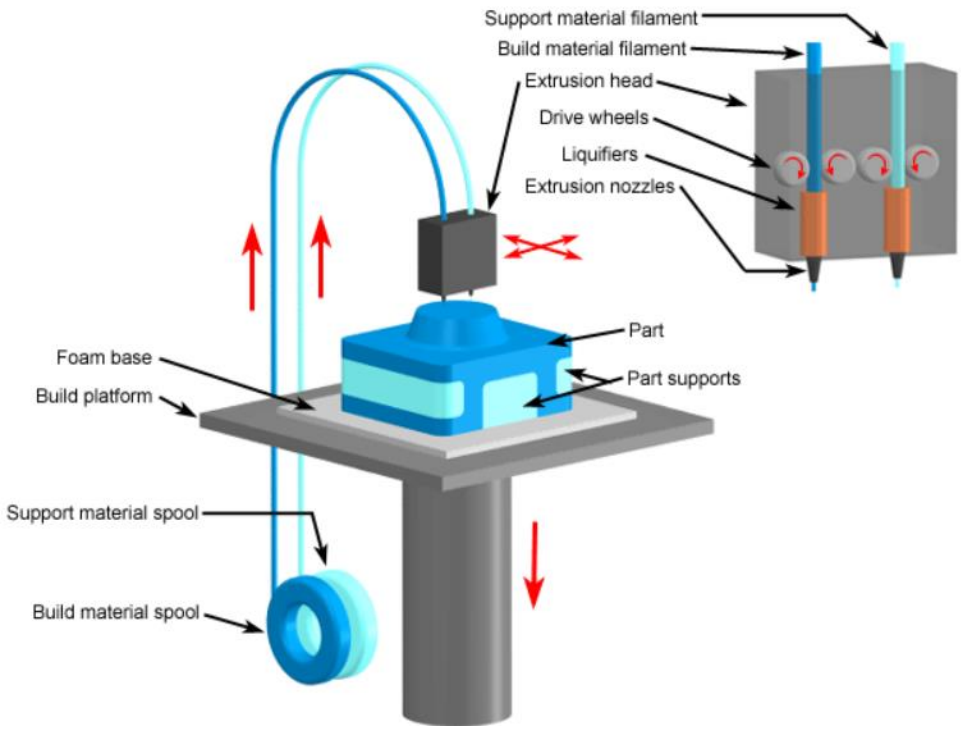

Figure 1- 1: Fused Deposition Machine

Picture from: http://www.custompartnet.com/wu/images/rapid-prototyping/fdm.png

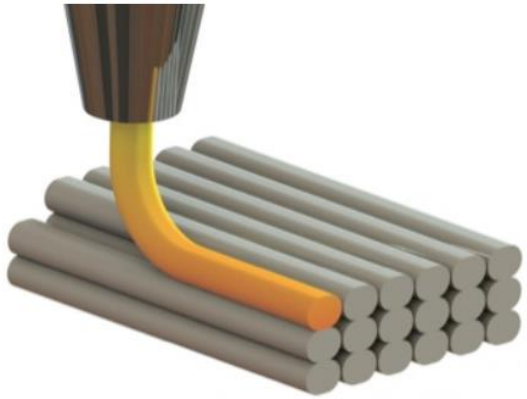

Figure 1- 2: Extrusion Nozzle and Filaments Layout

Picture From: **https://www.additive3d.com/extrusion-deposition-fused-deposition-modeling-fdm/**

FDM machines use 3D models from CAD tools, Computer tomography scans or magnetic resonance imaging scans to generate 3D objects. Then the 3D model is formatted in a CAD system to stereolithography format (STL). The 3D object in STL format then decomposed and sliced into horizontal layers. Some 3D objects need support structures during the print process. If support structure needed, then the support structure is modeled and sliced in the similar process. Other parameters are also defined the 3D printer software. Other parameters include: Nozzle speed, Tolerance, extruder temperature, Infill, gap and raster angle.

The direction at which the filaments are laid down on the platform is called raster angle. Raster angle can be between 0 degree and 180 degrees with respect to the X-axis of the printer. The gap is the distance between the center of adjacent filaments. The gap can be positive, negative and zero. Infill is defined as a percentage. Infill value is the fill percentage of an object.

1.6 ABS Material:

Acrylonitrile butadiene styrene (ABS) is a thermoplastic and amorphous polymer with good dimensional stability and toughness. ABS material is widely used in FDM process. ABS molecules are uncross-linked, and they exhibit glass transition temperature. Due to its amorphous nature ABS doesn't have a distinctive melting temperature.

When two polymeric objects are above glass transition temperature bonding formation occurs at their interface. At temperatures above the glass transition temperature, molecules have enough thermal energy for isometric rotational motion. Molecules rotate towards their preferred direction to reach the absorptive equilibrium. At higher temperature molecules have more rotational freedom, therefore, more molecular diffusion occurs at the interface.

1.7 Polymer Sintering process:

Bonding between adjacent filaments occurs due to polymer viscous sintering process. Polymer sintering is defined as the coalescence of polymeric particles due to the effect of surface tension.

Polymer sintering occurs at temperatures above the glass transition temperature for amorphous polymers, and for semi-crystalline polymers, it occurs at temperatures above the melting point of the polymer.

As shown in Figures 1-3 and 1-4, First interfacial molecular contacts are established at the contact points between the filaments, this stage of the sintering is called initiation [1] Then as long as the temperature of the filaments stays above the glass transition temperature, the filaments undergo deformation to reduce their total free surface. This stage of sintering is called Neck's

growth [1]. The longer the temperature stays above glass transition temperature at Neck's growth stage, the longer the interface becomes. Surface tension is the driving force in the neck's growth stage. [1]. Viscosity is the resistive force in polymer sintering. The sintering process continues until viscous forces and surface tension forces reach an equilibrium.

Sintering research has shown that small temperature changes or gradients during sintering process can change the sintering rate [1, 3, 15].Therefore, bonding quality and the strength of the bond are highly dependent on the thermal properties of the extruded polymer and the thermal history of filaments [3, 4, 16].

Experimental results have shown that the rate of the neck's growth stage for ABS polymers becomes negligible at temperatures below 200 ^{o}C. This temperature is called critical sintering temperature [6].

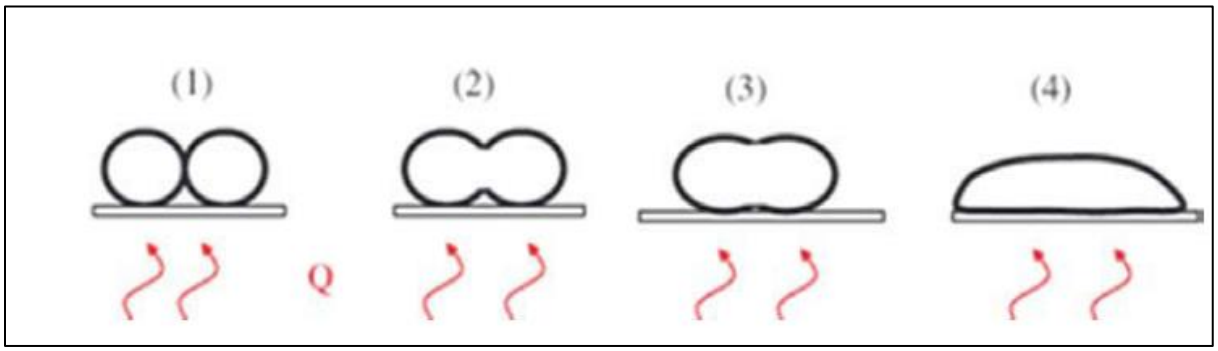

Figure 1- 3: (1)Initiation, (2) and (3) Neck's growth, (4) end of coalescence [1]

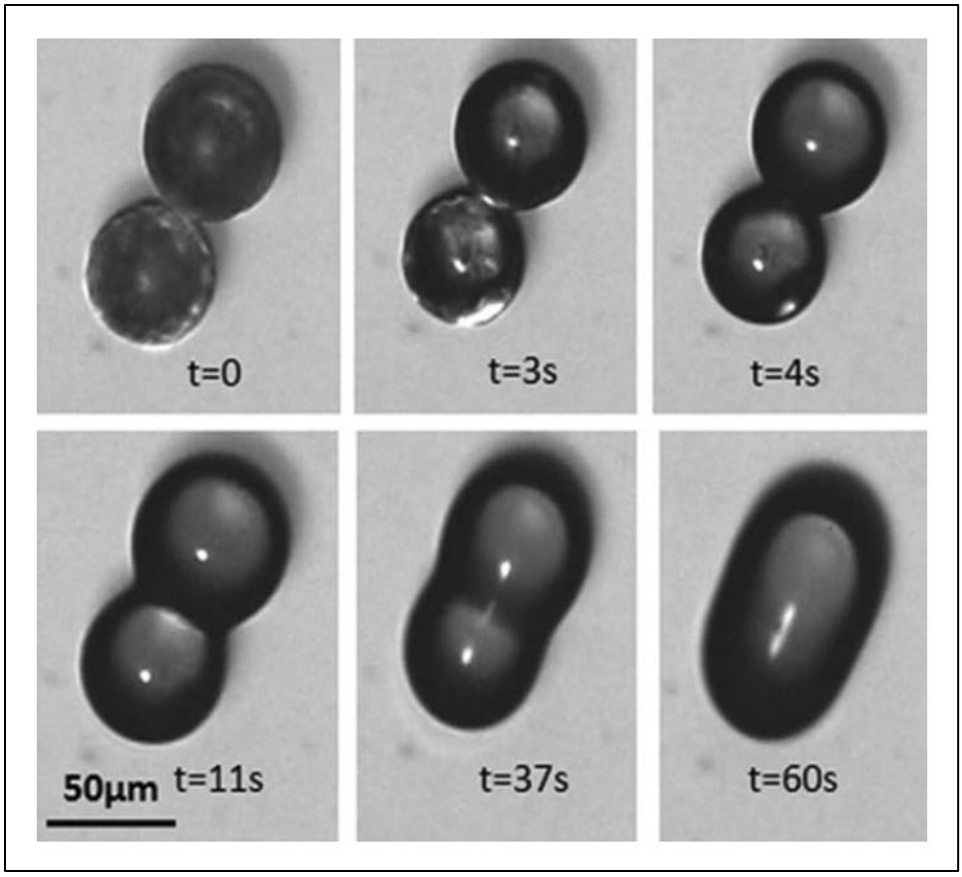

Figure 1- 4: Isothermal Polymer Sintering process. [1]

1.8 Fusion Mechanism through Molecular diffusion:

Understanding the rate of healing at the interface of filaments is of great importance, as it provides important details on the development of material properties between two polymers. Microscopic theory of molecular diffusion is used to study the healing rate and development of material properties in this research.

During the neck's growth stage as the interface between the filaments grows and becomes longer, polymer chain at the interface come in contact with each other and they begin to diffuse. The rate of the diffusion process depends on the molecular weight, temperature and contact

pressure between the filaments. Diffusion process takes place at temperatures above glass transition temperature for amorphous polymers.

Higher temperature at the interface during the sintering process results in stronger molecular diffusions and stronger bonding properties between filaments [3], as polymer chains at the interface have higher thermal energy that facilitates their motions.

Polymer diffusion process consists of 3 stages [17] as shown in Figure 1-5. At the wetting stage molecules come in contact across the interface. Then during the diffusion state molecules move and form molecular bridges across the interface. The third stage is randomization where the interface between the two polymer disappears and maximum mechanical properties are recovered at the interface.

The molecular diffusion in the FDM process is non-isothermal due to the transient temperature nature of the FDM process.

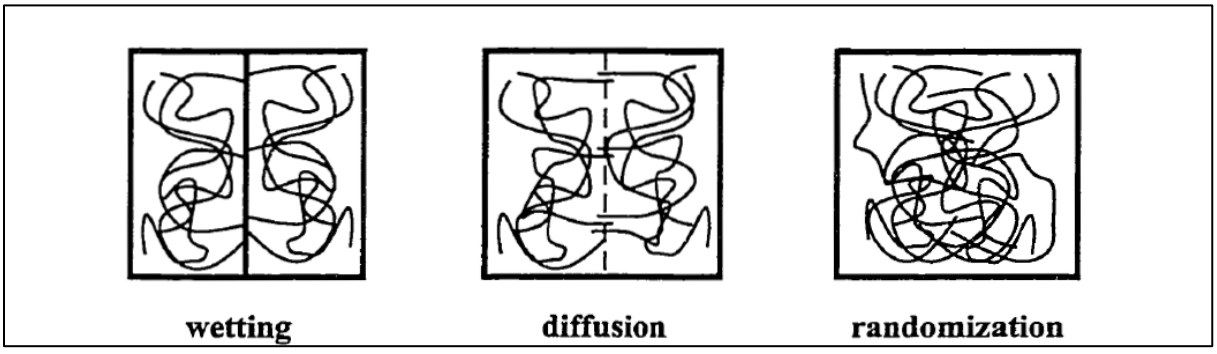

Figure 1- 5: Three stage of molecular bonding at Interface [3]

1.9 Thermal Properties:

Thermal properties of the ABS P400 were measured by Rodrigues [3]. Thermal conductivity and specific heat were reported as a function of temperature.

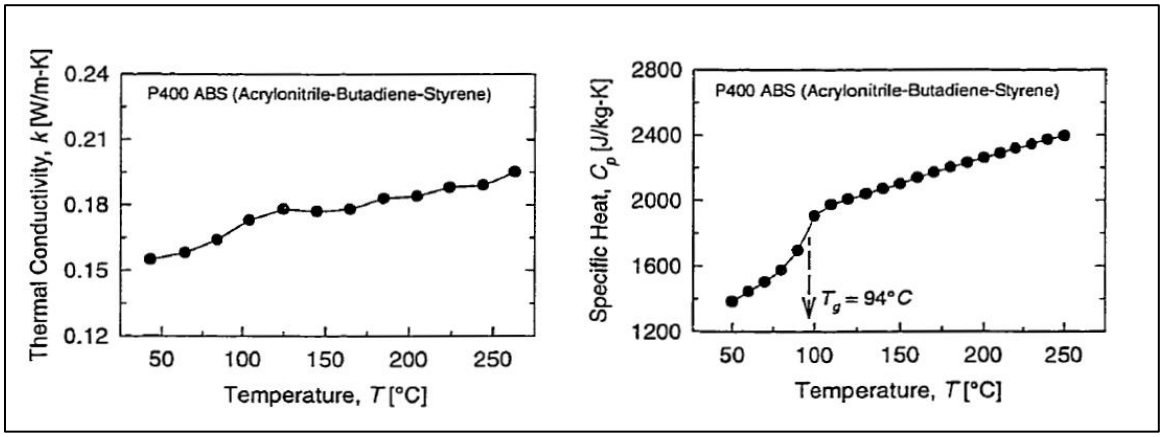

Figure 1- 6: Thermal conductivity and specific heat for ABS P400 [3]

1.10 Glass Transition:

Glass transition temperature is the temperature at which amorphous polymers transit into a viscous and rubbery state from a hard and glassy state, as the temperature increases. Glass transition temperature of ABS polymer has been reported by Rodriguez [3] as 94 ^{o}C.

1.11 Dynamic Viscosity:

Dynamic viscosity was determined using a Haake RS150 rotational rheometer [15]

$$\mu = 5100\, e^{-0.056\,(T-503)} \tag{1.1}$$

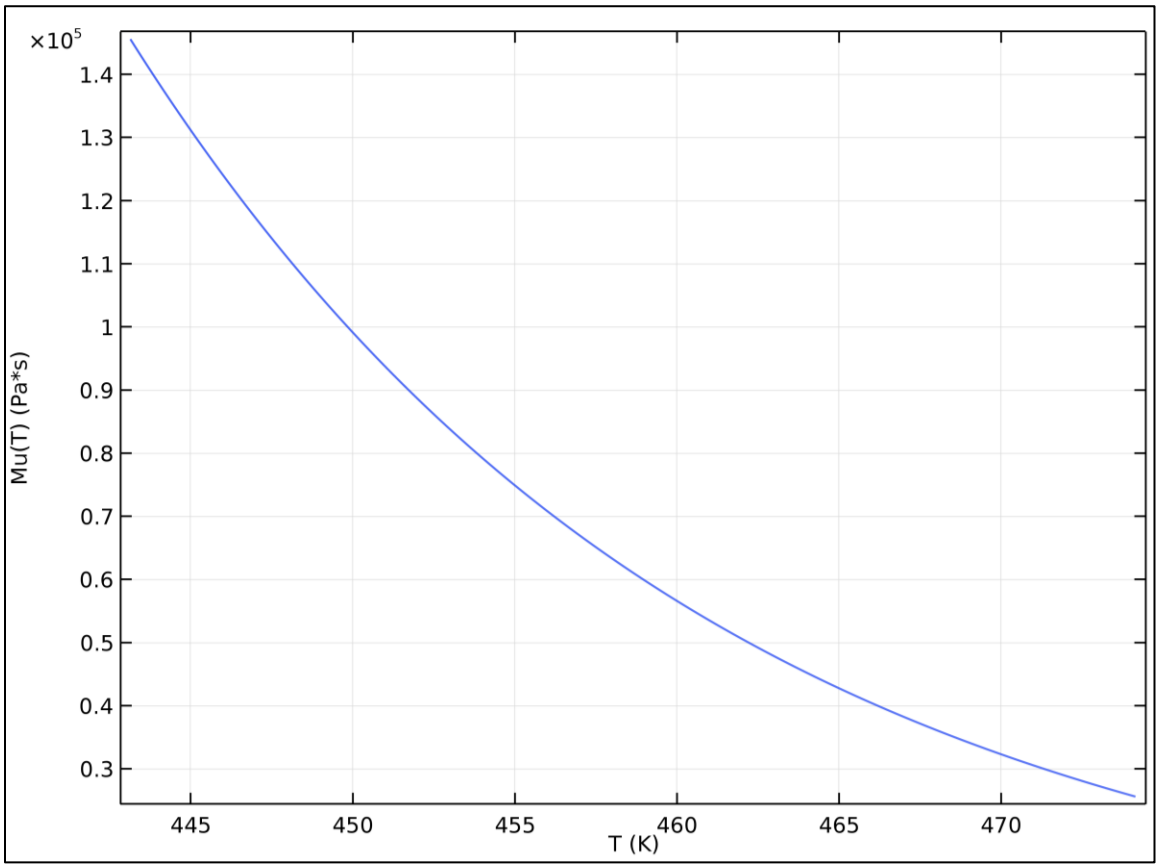

Figure 1- 7: Dynamic Viscosity of ABS P400 As a Function of Temperature

1.12 Surface Tension:

Surface tension function was defined as below per [15]

$$\tau = 0.029 - 345 * 10^{-4} * (T - 513) \tag{1.2}$$

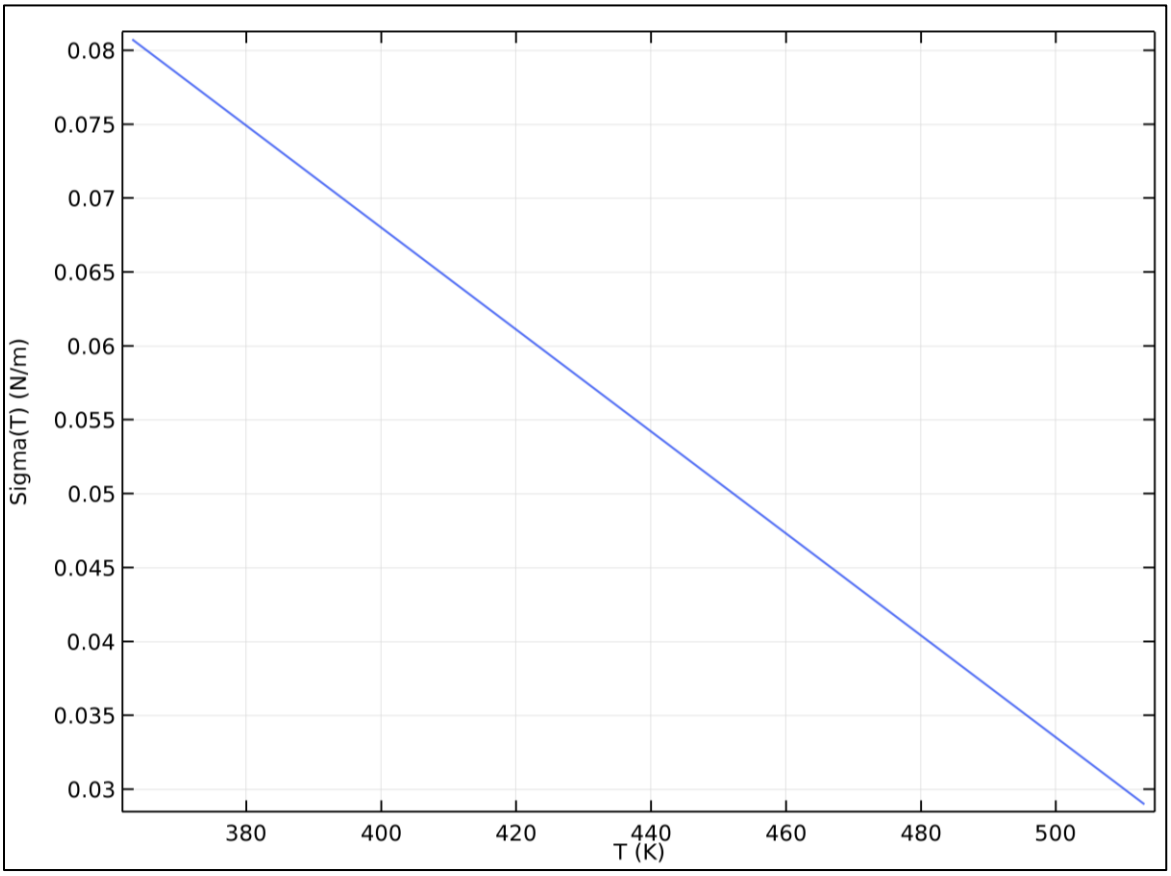

Figure 1- 8: Surface Tension of ABS P400 As a Function of Temperature

Chapter 2:

Numerical Modeling of Non-Isothermal Polymer Sintering

2.1 Methodology/approach:

Most of the polymer sintering reaserch presented in the literature are based on the Pokluda [5] isothermal sintering model.

$$\frac{d\theta}{dt} = \frac{\Gamma}{a_o \mu} \frac{2^{-5/3} \cos\theta \sin\theta (2 - \cos\theta)^{1/3}}{(1 - \cos\theta)(1 + \cos\theta)^{1/3}} \tag{2.1}$$

Where $\theta = sin^{-1}(\frac{\gamma}{a})$, μ is viscosity, a is initial radius of a particle and τ is surface tension.

This model is useful for isothermal models; however, for non-isothermal models using this method results in erronious results as the temperature, viscosity and surface tension change during the sintering process in FDM machines.

The fused deposition process is a highly nonlinear process with material and geometric nonlinearities. A detailed model of this process should include Thermal and Fluid analysis. A multiphysics model of the fused deposition process is presented in this chapter

2.2 Transient Heat analysis:

To capture the transient heat profile and the temperature gradient across the filament's cross sections, a 2D finite element model of the process was developed. The FDM process is a dynamic process where material is constantly added and the boundary conditions of the filaments change during the process.

In order to account for the change in the boundary conditions of the filaments during the process, the transient heat analysis section of the model was defined in two steps. The first step includes the transient heat analysis of the first filament before the adjacent filament is printed,

shown in Figure 2-1a. The second step includes the transient heat analysis of both filaments with new boundary conditions as the second filament is printed, shown in Figure 2-1b.

The initial temperature of the filament in the first step was set equal to the extrusion temperature. The first step was analyzed until the second filament is printed (t = 2.L / Unozz). The second step uses the last nodal temperature of the first step for the first filament's initial temperature and sets the initial temperature of the second filament equal to the extrusion temperature.

The change in the boundary conditions of filaments during the simulation is illustrated in Figure 2-1.

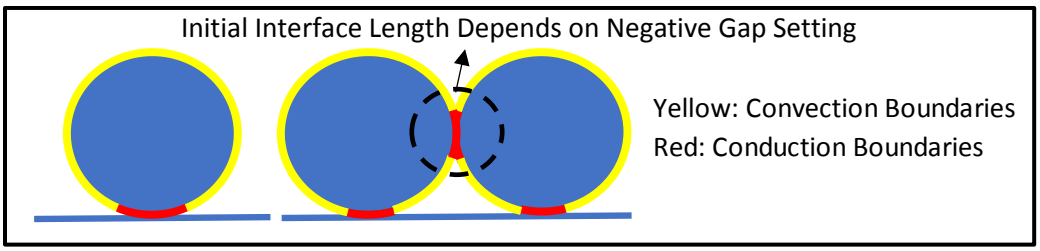

Figure 2- 1: A) First Filament B) First and Second Filaments

Elliptical linear, nonhomogeneous partial differential equation solved in this model is explained below:

$$\rho C_P \frac{\partial T}{\partial T} - \nabla.(k\nabla T) = Q \tag{2.2}$$

k , C_P ,ρ, and Q denote thermal conductivity, specific heat, density, and heat sources, respectively. Thermal conductivity , (k), and specific heat, (C_P), are functions of temperature as reported by Rodriguez [3]

$$k\left[{}^{W}/_{m.C}\right] = 2\times T\times 10^{-4} + 0.14 \quad (2.3)$$

$$C_p\left[{}^{J}/_{kg.C}\right] = 5\times T + 1150 \quad (2.4)$$

$$\rho = 1050\ kg.m^{-3} \quad (2.5)$$

Convective cooling boundary condition:

Convective heat flux on the boundaries in contact with air is modeled as temperature difference between fictitious thermal boundary layers. The convective heat flux is described by the below equation:

$$q = h(T_{ext} - T) \quad (2.6)$$

h denotes convective heat transfer coefficient. The $\overline{N_{UD}}$ average free convection heat transfer coefficient was used for determining the value of convection coefficient.[18]

$$h = \frac{k}{D}\left(0.6 + \frac{0.387\mathrm{Ra}_D^{1/6}}{\left(1+\left(\frac{0.559}{\mathrm{Pr}}\right)^{9/16}\right)^{8/27}}\right)^2 \quad (2.7)$$

$$\mathrm{Ra}_D = \frac{g\alpha_p\rho^2 C_p|T - T_{\mathrm{ext}}|D^3}{k\mu} \quad (2.8)$$

$R_{a_D} and\ Pr$ are the Rayleigh and Prandtl dimensionless numbers. g is acceleration of gravity, $\propto_p$ is Air's coefficient of thermal expansion, T is the temperature of the filament, T_{ext} is the envelope temperature, C_P is the heat capacity of Air in constant pressure, D is the Diameter of the Filament, μ represents the air's dynamic viscosity, k is thermal conductivity of Air, and ρ is the density of air.

2.3 Computational Fluid Dynamic Analysis:

To model the non-isothermal viscous sintering process that occurs between adjacent filaments while the temperature is above the glass transition temperature, a CFD analysis was coupled with the transient heat transfer analysis.

2.4 Stokes Creeping Flow:

Sintering process is a slow process with Reynolds number well below unity. Therefore, the viscous forces dominate the inertia forces. With Inertia forces being small compared to the viscous forces, the inertia forces can be neglected in the analysis when the Navier-Stoks equations are solved. The reduced Navier-Stoks equations are called Stokes creeping flow.

The numerical simulation is carried out by solving stokes creeping flow equation for the geometry. Backward Euler time step along with arbitrary Lagrangian-Eulerian formulation is employed to predict the geometry deformation for the next time step. In each time step, the temperature from the transient heat analysis is used to update the material properties that are dependent on temperature.

$$0 = \nabla.[-p\,\boldsymbol{I} + \tau] + \boldsymbol{F} \tag{2.9}$$

$$\nabla.u = 0 \tag{2.10}$$

Where p is pressure, τ is viscous stress tensor, F is Volume force vector and u denotes velocity vector. viscous stress tensor is defined as below:

$$\tau = 2\mu\boldsymbol{S} - \frac{2}{3}\mu(\nabla.u)\boldsymbol{I} \tag{2.11}$$

S is the strain-rate tensor

$$\boldsymbol{S} = \frac{1}{2}\times(\nabla u + (\nabla u)^T) \tag{2.12}$$

2.5 Arbitrary Lagrangian-Eulerian Method [19, 20]:

To accurately evaluate the change in the surface between the two filaments and predict the amount of neck's growth the ALE (arbitrary Lagrangian-Eulerian) method is employed.

ALE method is an intermediate between Lagrangian and Eulerian coordinate system. In the ALE, when the spatial coordinate system is mapped with material coordinate system and follows the material deformation, a Lagrangian coordinate system is recovered. However, when the map is an identity map, an Eulerian coordinate system is recovered.

The elements at the interfaces are deformed to account for the change in the surface and growth of the neck between filaments. The solver uses boundary displacement by solving mesh displacement equations.

For the 2D domain that is used for sintering simulation, we can relate the spatial coordinate (deformed mesh coordinates) to the original unreformed mesh (material frame) using a function:

$$\text{Spatial Coordained} = (x , y) \tag{2.13}$$

$$\text{Material Coordinate} = (X , Y) \tag{2.14}$$

$$x = x (X , Y , t) \quad y = y (X , Y , t) \tag{2.15}$$

Each node's spatial coordinate is defined by the above functions. These functions are either explicit or are the solutions to the mesh smoothing equations.

$$\text{Spatial coordinate } x = [x, y] \tag{2.16}$$

$$\text{Material coordinate } X = [X, Y] \tag{2.17}$$

$$\mathbf{x} = f(\mathbf{X}, t) \tag{2.18}$$

f is a vector values function and t is time. When f assigned as a unit map, the ALE formulation becomes Eulerian.

Then the stokes creeping flow equations along with heat transfer equations are solved in the spatial frame. By solving the equations over the spatial frame, the movement of the interface is accounted for.

2.6 External Fluid Boundaries:

Since the viscosities of the two fluids (Air and Polymer) are significantly different. With polymer having much higher viscosity than the Air. Therefore, we can neglect the viscosity term in the total stress equations.

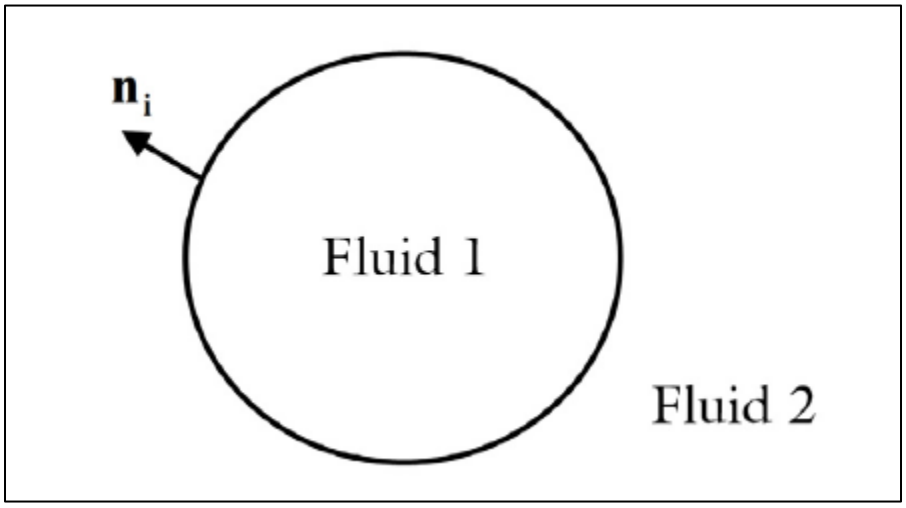

Figure 2- 2: Two Phase Fluid and Normal Vector [21]

The boundary conditions applied at the two-immiscible fluid interface with one fluid having significantly lower viscosity than the other is defined as below:

$$n_i . \tau_i = -p_{ext} . n_i + f_{st} \quad (2.19)$$

$$\boldsymbol{u}_{mesh} = (u_1 . n_i) n_i \tag{2.20}$$

f_{st} denotes for force per unit area due to the surface tension.

τ_i denote for the total stress tensor in the domain.

$\boldsymbol{u}_{mesh}$ denotes velocity of the mesh at the interface.

n_i is the normal of interface.

The second fluid, air around the filaments, does not affect the velocity field of the first liquid, polymer, therefore the second fluid is not needed to be explicitly modeled in the simulation. The second fluid only contributes to the equations through the pressure term, P_{ext}.

2.7 Surface Tension force:

The force tension force is defined as below:

$$f_{st} = \sigma(\nabla_s . n_i) n_i - \nabla_s \sigma \tag{2.21}$$

∇_s is the surface gradient operator. σ denotes surface tension at the interface.

$\nabla_s . n_i$ is for the mean curvature of the surface defined by

$$\kappa = -\nabla_s . n_i \tag{2.22}$$

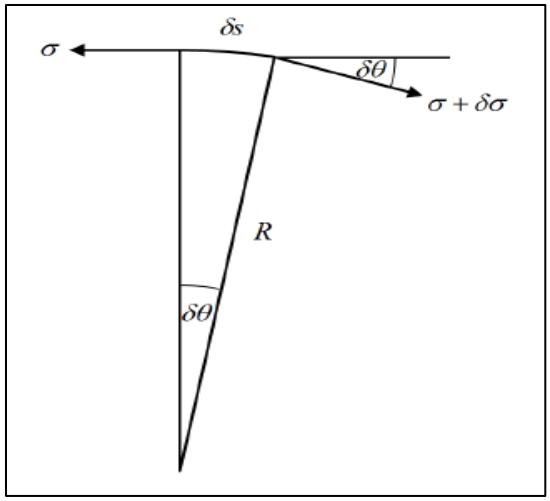

Figure 2- 3: Surface tension forces acting on a surface element [22]

2.8 Normal Force Due to Surface Tension:

The first term, $\sigma(\nabla_s . n_i)n_i$, is the normal force per unit area acting on the boundary resulted by surface tension vector.

For the 2D analysis performed in this research, the elements residing at the surface of the filaments the normal force per unit area F_n is the limit of $\delta s \to 0$ as shown below:

$$F_n \delta\sigma = (\sigma + \delta\sigma)\sin(\delta\theta) \tag{2.23}$$

$$F_n R\delta\theta = (\sigma + \delta\sigma)\sin(\delta\theta) \tag{2.24}$$

$$F_n \to \frac{\sigma}{R} \tag{2.25}$$

for two dimensional models, the mean curvature is $\kappa = \frac{1}{R}$; therefore, $-\nabla_s . n_i = \frac{1}{R}$

2.9 Tangential force Due to Surface Tension:

The second term in the surface tension equation, $\nabla_s \sigma$, is the tangential force per unit area applied to the boundary.

The tangential force per unit area, F_t, is obtained from the force balance along δs as $\delta s \to 0$

$$F_t \delta s = (\sigma + \delta\sigma)\cos(\delta\theta) - \sigma \tag{2.26}$$

$$F_t \to \frac{(\sigma + \delta\sigma) - \sigma}{\delta s} \tag{2.27}$$

2.10 Contact Angle:

In order for the fluid to maintains a constant contact angle at the 3-phase boundary, a force term is added at the contact point. The surface tension force per unit length is in equilibrium with reacting force per unit length at the surface, F_n, and forces generated by surface energies of the fluids, γ_{s1} and γ_{s2}. Contact angle reported in the literature for ABS material is 80~82 degrees.

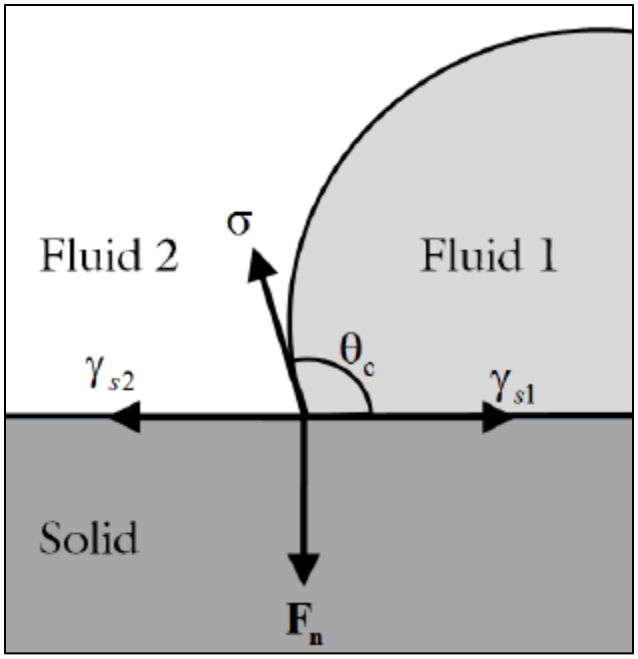

Figure 2- 4: Forces acting at the contact point [21]

2.11 Results and Discussion:

Filament's diameter print speed, extrusion temperature, envelope temperature, viscosity, surface tension and gap setting were identified as important parameters affecting the quality of the bond formation between filaments.

As shown in figure 2-5, different parameter setting affects thermal history of filaments significantly. Initial temperature at the filament interface as shown in figure 2-5, varies from 252 ^{o}C to 184 ^{o}C depending on the printer's parameter setting. This variation in thermal energy at the interface results in differential healing and strength development at the interface. To optimize the degree of healing and strength development at the interface, maximum wetting length, and maximum initial temperature is required. The maximum wetting length is defined by the gap

setting parameter and the maximum temperature at the interface achieved using maximum print speed, filament diameters, extrusion temperature and envelope temperature.

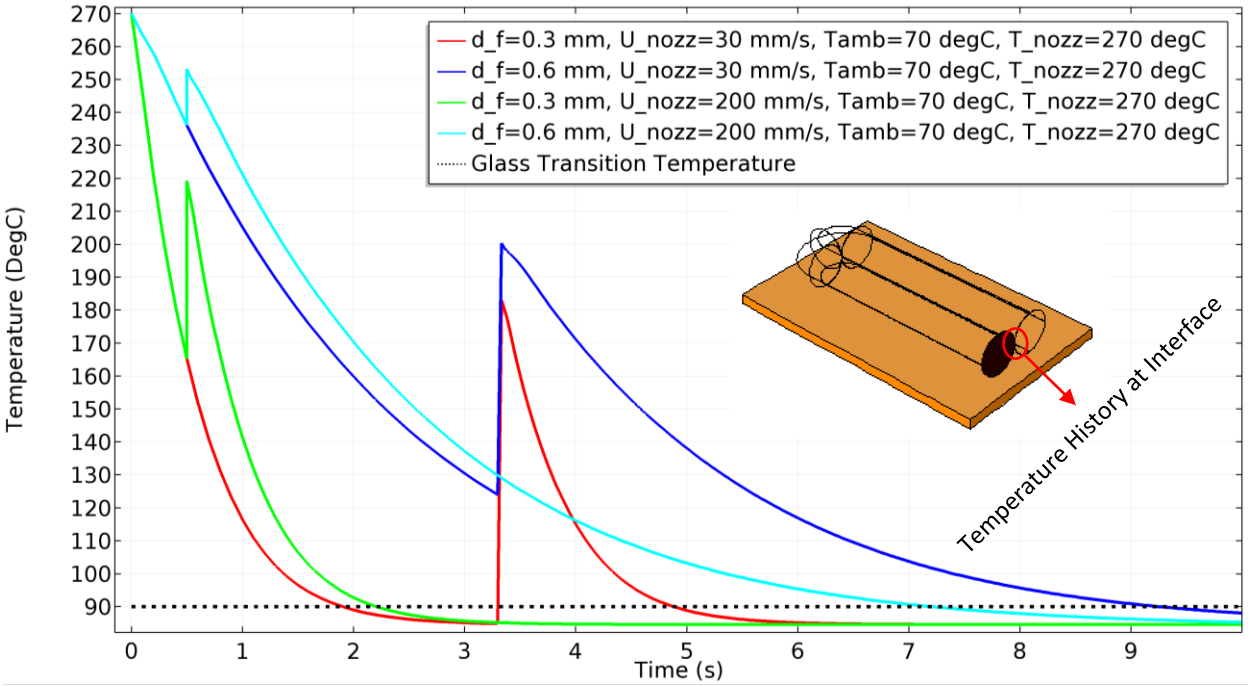

Figure 2- 5: Thermal History of Filaments with Different Print Setting

2.12 Filament Diameter:

The diameter of filaments is the most important variables affecting the interfacial properties. The numerical results show that larger diameter filaments experience higher initiation temperature and longer neck's growth time. Therefore, stronger interface bonding occurs between filaments due to stronger molecular diffusion and larger interface length. This is mainly due to the higher thermal capacity of the larger filaments. Larger diameters filaments, however, are not desirable as the surface finish and dimensional tolerancing of the FDM objects are negatively affected.

Figure 2-6 illustrates temperature history of different filament's diameter. The 0.3 mm filament has initiation temperature of 185^{o}C and 2 sec for neck's growth. The 0.6 mm filament has initiation temperature of 208^{o}C and 6 sec for neck's growth.

This significant increase in the initiation temperature and neck's growth time explains the experimental results obtained by B. Rankouhi and his colleague [23]. Rankouhi's experimental results show that the lateral ultimate strength of the 0.4 mm filaments is 4.38 times higher than the 0.2 mm filaments. This significant increase in the lateral strength of the filaments is attributed to the significantly higher initiation temperature and longer molecular diffusion time [3]and neck's growth between the filaments.

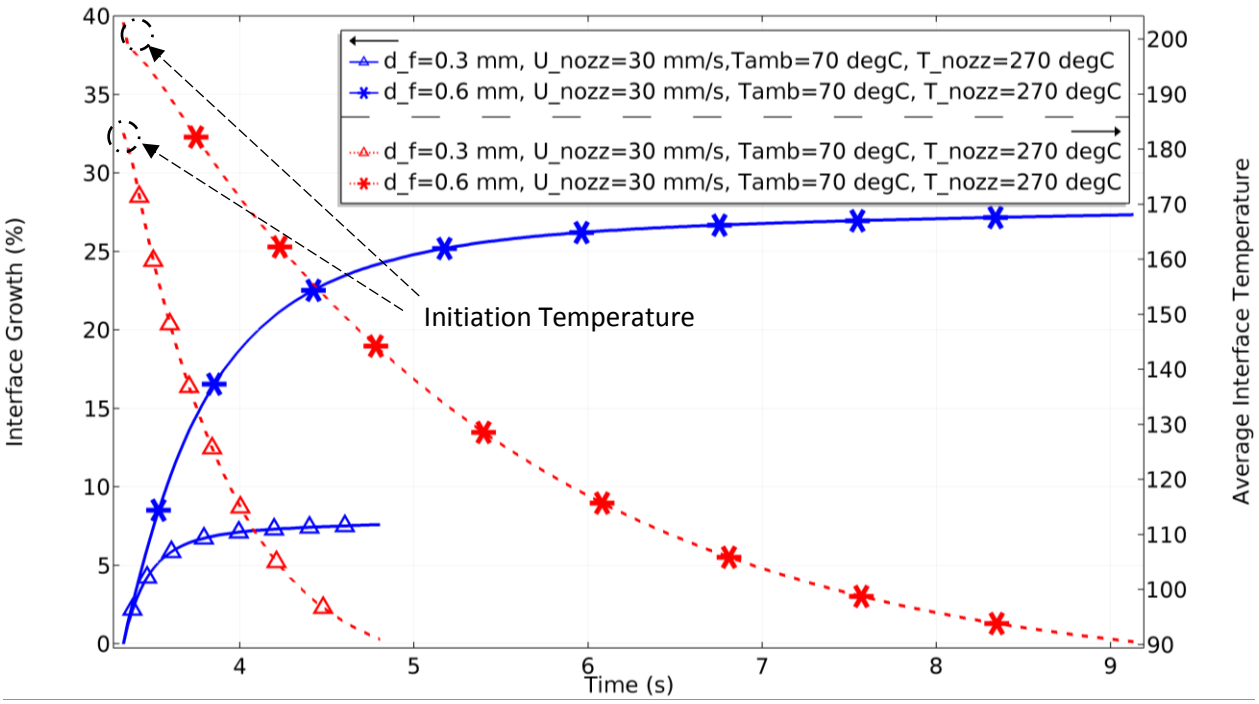

Figure 2- 6: Temperature History and Neck's Growth Rate of Different Filament Diameters

2.13 Print Speed (Nozzle Speed):

Print speed is the speed at which filaments are printed and laid down side by side. The higher the print speed is, the less time it takes for the filaments to lose heat, hence higher initiation temperature. As a result, stronger molecular interface and interfacial properties develop between filaments.

Figure 2-7 illustrates the importance of print speed in the temperature history of filaments interface. Filaments printed with speed of 200 mm/s have 22% higher initiation temperature and 23% longer neck's growth time than filaments printed with speed of 30 mm/s. Increase in print speed becomes more important for smaller diameter filaments as it can increase the interface temperature above the critical sintering temperature of 200^{o}C [6].

Reducing the length of the filaments also has the same effect as increasing the speed of the nozzle. Change of the print strategy from longitudinal to lateral for rectangular specimens results in shorter filaments and higher initiation temperature. This effect has been confirmed by experimental observations.[15, 16]

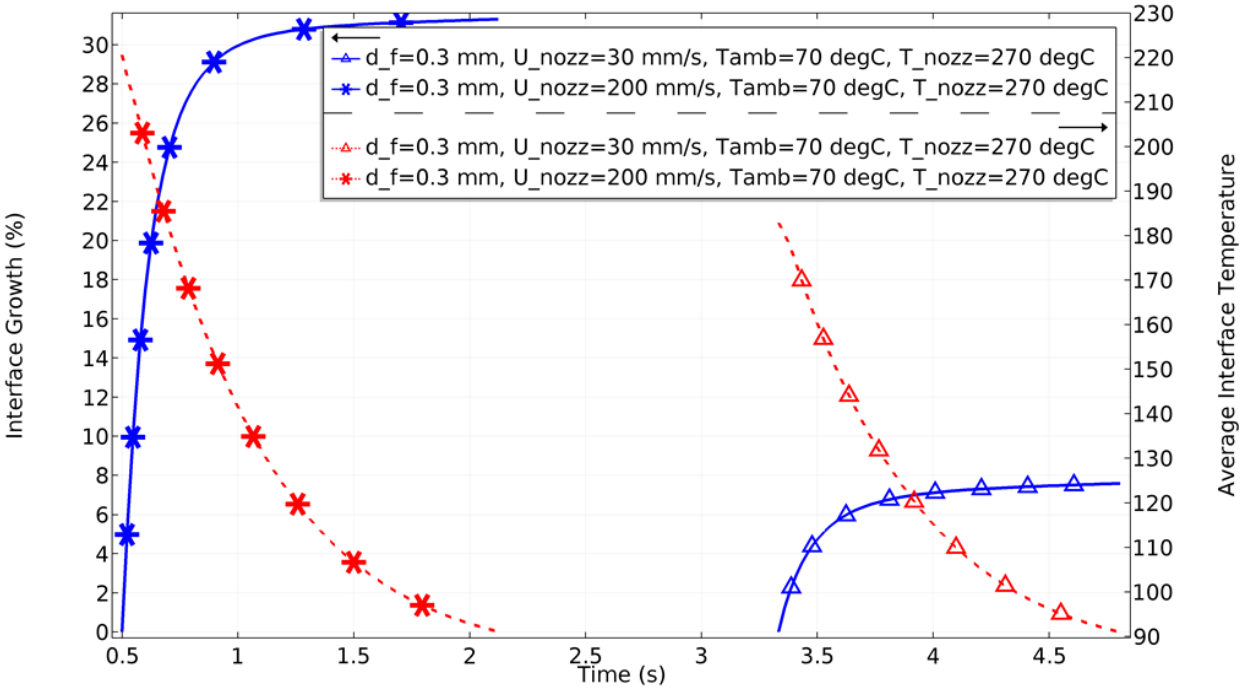

Figure 2- 7: Temperature History and Neck's Growth Rate of Filaments with Different Nozzle Speeds

2.14 Extrusion temperature:

Extrusion temperature of the filaments is the temperature at which the filaments are extruded onto the platform. This temperature defines the initial thermal energy of the filaments. Higher extrusion temperature results in higher initiation temperature and longer sintering time as shown in Figure 2-8.

The Higher extrusion temperature is desirable for achieving improved interfacial properties. At higher extrusion temperature viscosity of the filaments are lower, therefore, neck's growth rate is higher.

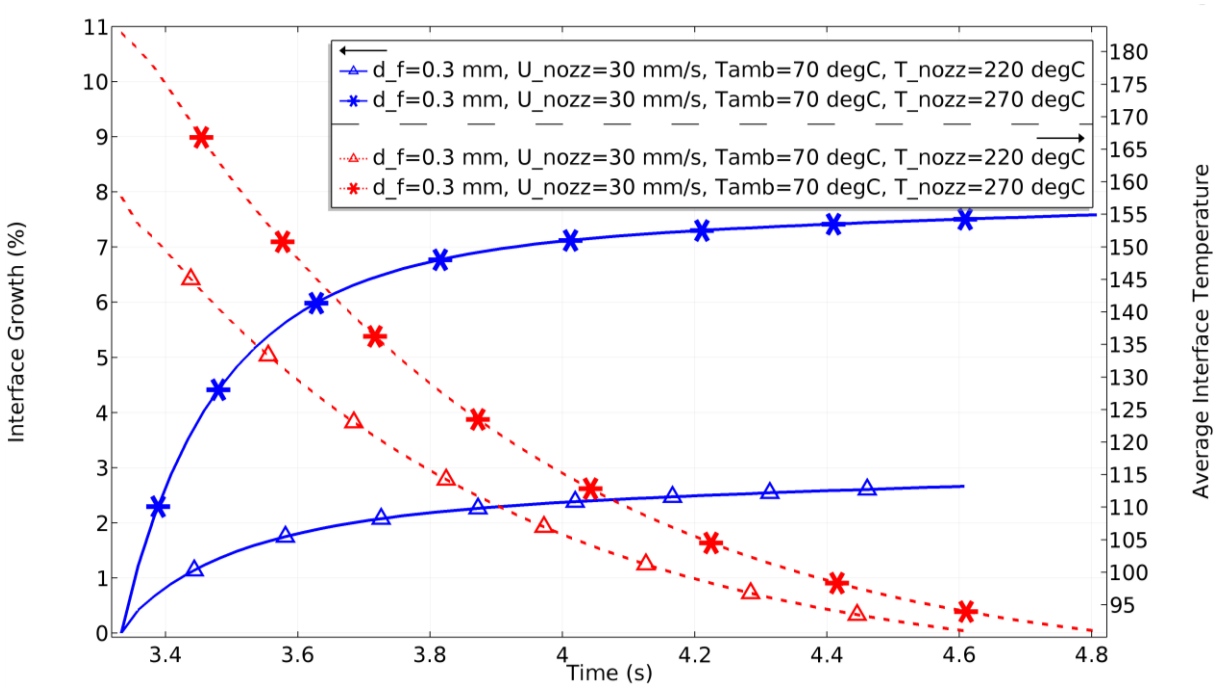

Figure 2- 8: Effect of Extrusion Temperature and Neck's Growth Rate on Thermal History of Filaments

2.15 Envelope temperature:

Envelope temperature is the temperature of the envelope inside the printer. Envelope temperature defines the lowest temperature limit for filaments, therefore, it has an important effect on the convection and cooling rate of filaments.

As illustrated in Figure 2-9, the envelope temperature increases the necks growth time by lowering cooling rate of filaments.

Numerical simulation results indicate that the envelope temperature should be set slightly below the glass transition temperature of the filaments. Figure 2-8 and 2-9 confirm the results of the study done by C.Bellehumeur [6] that the effect of envelope temperature in the early stage of cooling is less important than the extrusion temperature.

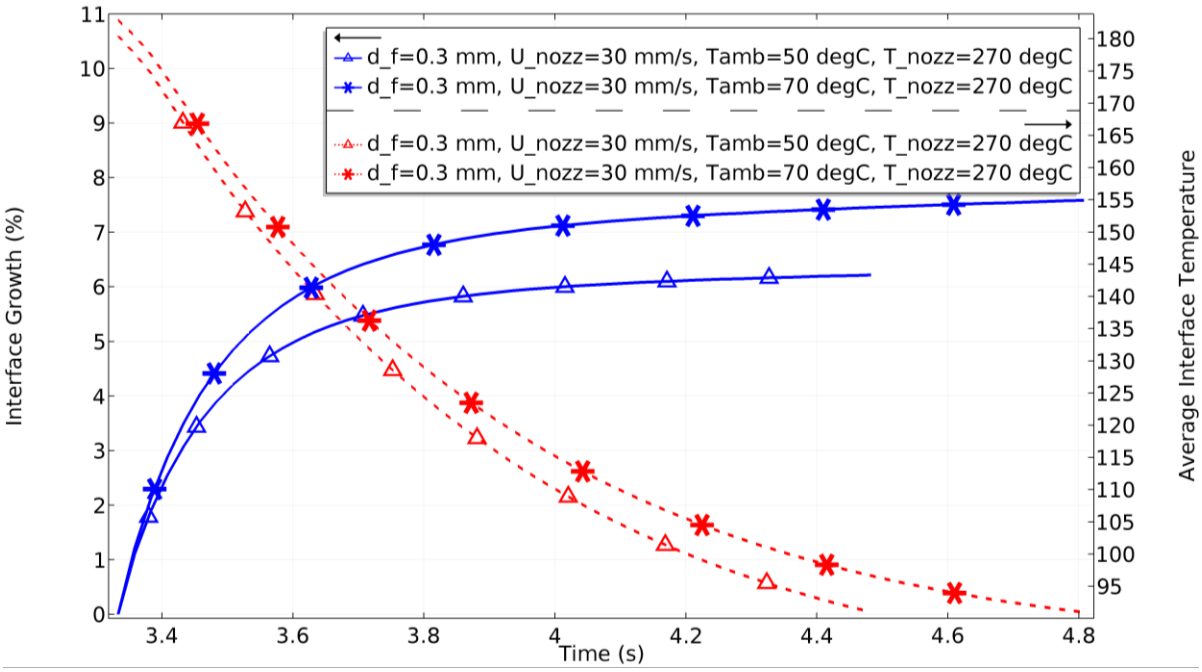

Figure 2- 9: Effect of Envelope Temperature on Thermal History and Neck's Growth Rate of Filaments

2.16 Viscosity and Surface Tension:

Viscosity and its sensitivity to temperature were observed to have a significant effect the neck's growth rate. The lower zero shear viscosity and the less sensitivity it has to temperature change result in longer growth of neck between filaments.

The driving force in sintering process is surface tension and the resistive force is a viscous force. Neck's growth continues until these two forces reach to an equilibrium. Therefore, increasing the surface tension of filaments helps in improving the length of the neck between adjacent filaments. There are some techniques proposed in the literature for increasing surface tension of liquids. There needs to be more research to evaluate the effect of the techniques proposed in the literature on the surface tension of ABS polymers.

2.17 Gap Setting:

Gap setting defines the distance between the adjacent filaments center line, (C.C.D). The negative gap between filaments increases the initial contact area between filaments. Numerical simulation results show that gap settings from negative 1 percent to negative 10 percent has no significant effect on the lateral temperature distribution of filaments. However, it was observed that higher negative gap setting increases the initial contact length and results in longer neck's growth between filaments. The longer initial contact length also results in stronger molecular diffusion as the larger portion of the interface experiences high initiation temperature.

Experimental results reported in the literature did not account for the effect of the gap setting in the formation of initial interface and development of neck between filaments. However, as shown in Figure 2-10 and 2-11, the gap setting can significantly affect the initial interface length of the filaments.

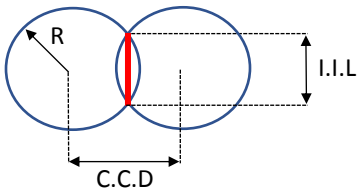

Figure 2- 10: Negative airgap setting introduces an initial interface (I.I) by reducing the Center to Center Distance (C.C.D) between the filaments.

Length of the initial interface (I.I.L) between the filaments calculated using the following formula:

$$I.I.L = 2\times r\times \cos\left[\frac{\pi}{2} - \cos^{-1}\left(\frac{r-d}{r}\right)\right] \quad (2.27)$$

$$d = \frac{r \times gp}{100} \tag{2.28}$$

Where r is the radius of the filament and gp denotes the negative gap percentage.

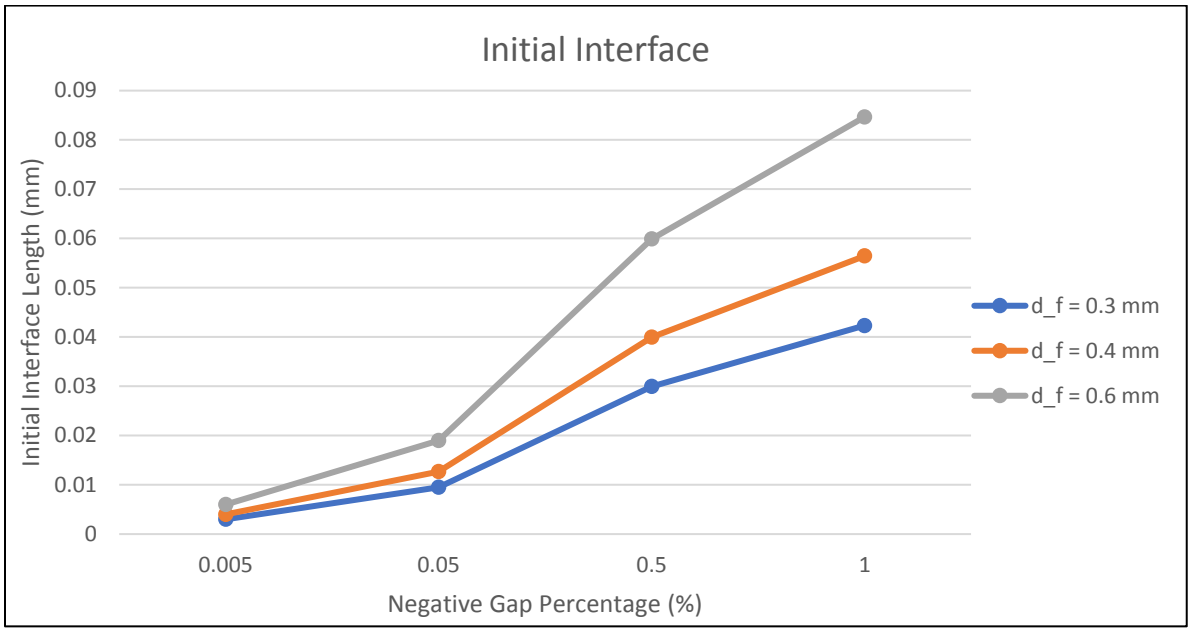

Figure 2- 11: Negative Gap percentage and Initial Interface Length

Figures 2-10 and 2-11 show the significance of the negative gap setting on the development of the interfacial properties of the filaments. As shown on the figures, the change in negative gap setting from 0.005% to 0.5% results in a negligible increase of 0.001 mm in the necks growth during the sintering phase; However, the change in initial interface length becomes significant. With the 0.005% gap setting the final length of the interface is 0.019 mm compared with 0.5% gap setting final length of 0.075 mm.

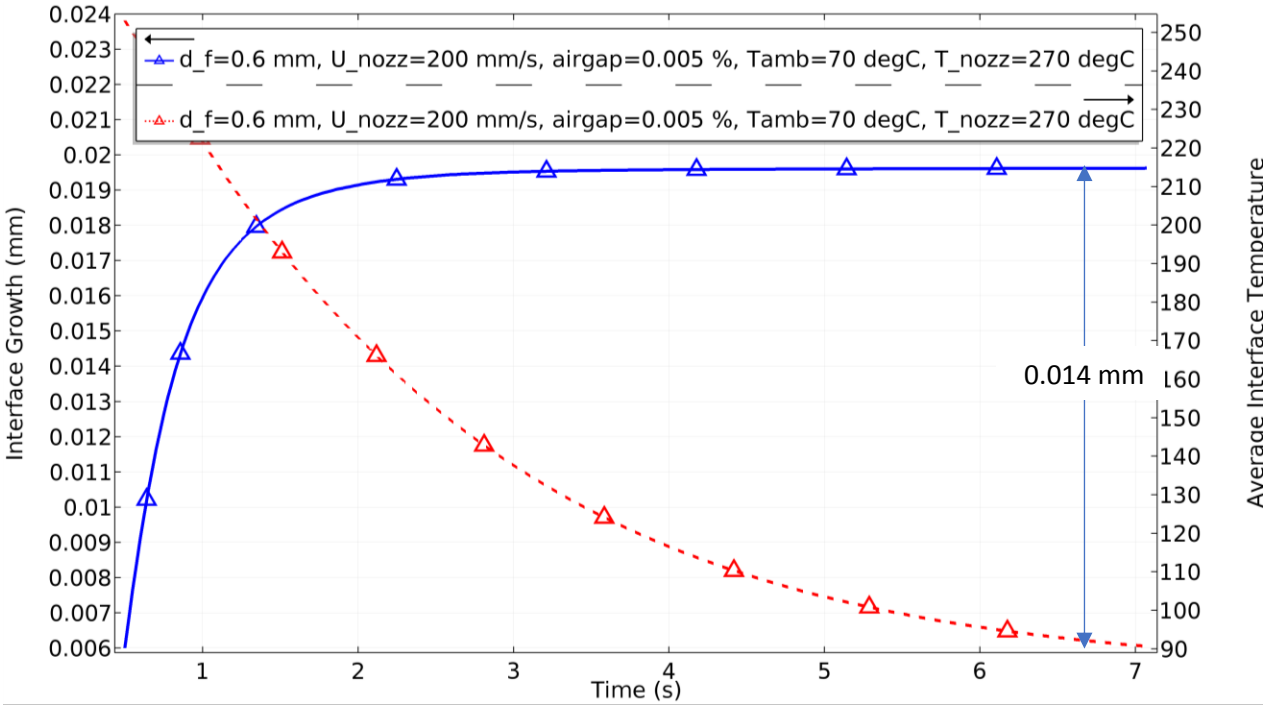

Figure 2- 12: Necks Growth Rate with 0.005% Negative Gap Setting

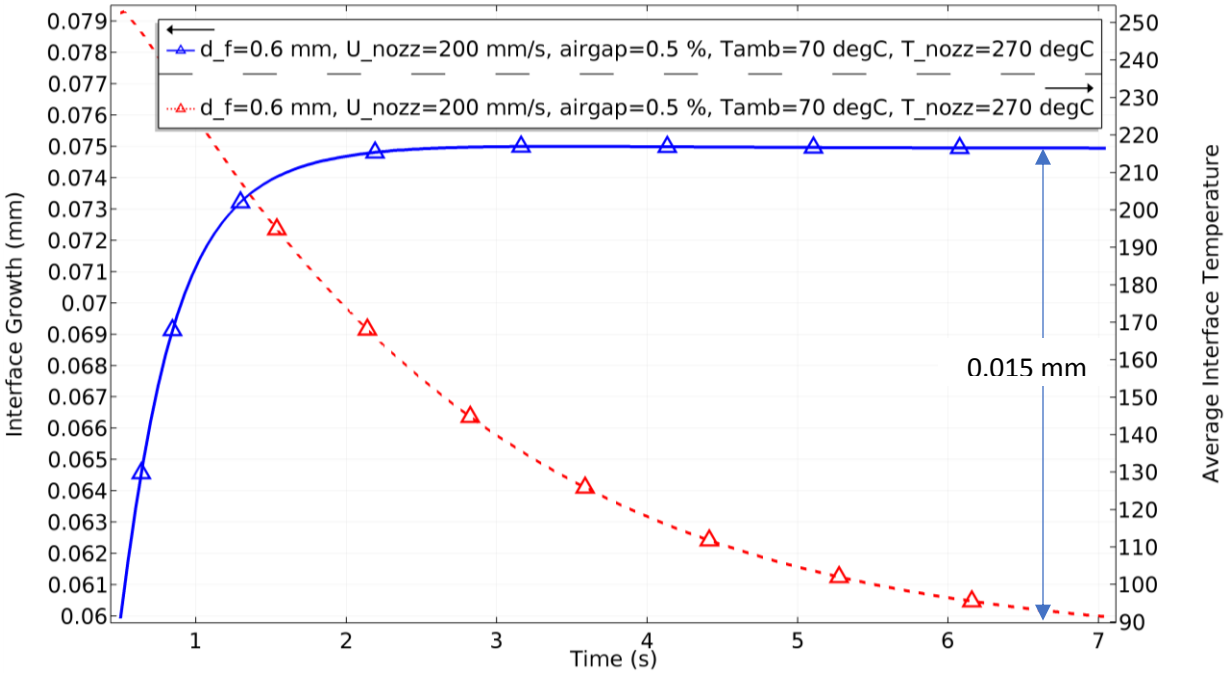

Figure 2- 13: Neck's Growth Rate with 0.5% Negative Gap Setting

Figures 2-14 and 2-15 show the importance of gap setting in the bond formation between adjacent filaments.[4, 24]

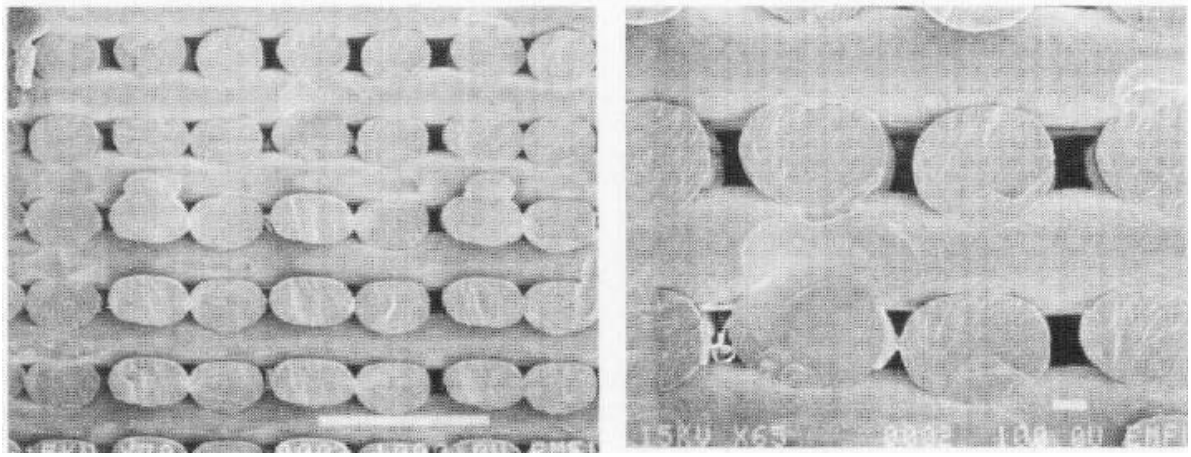

Figure 2- 14: Excessive Gap Between Filaments Results in Poor Bonding at Interface

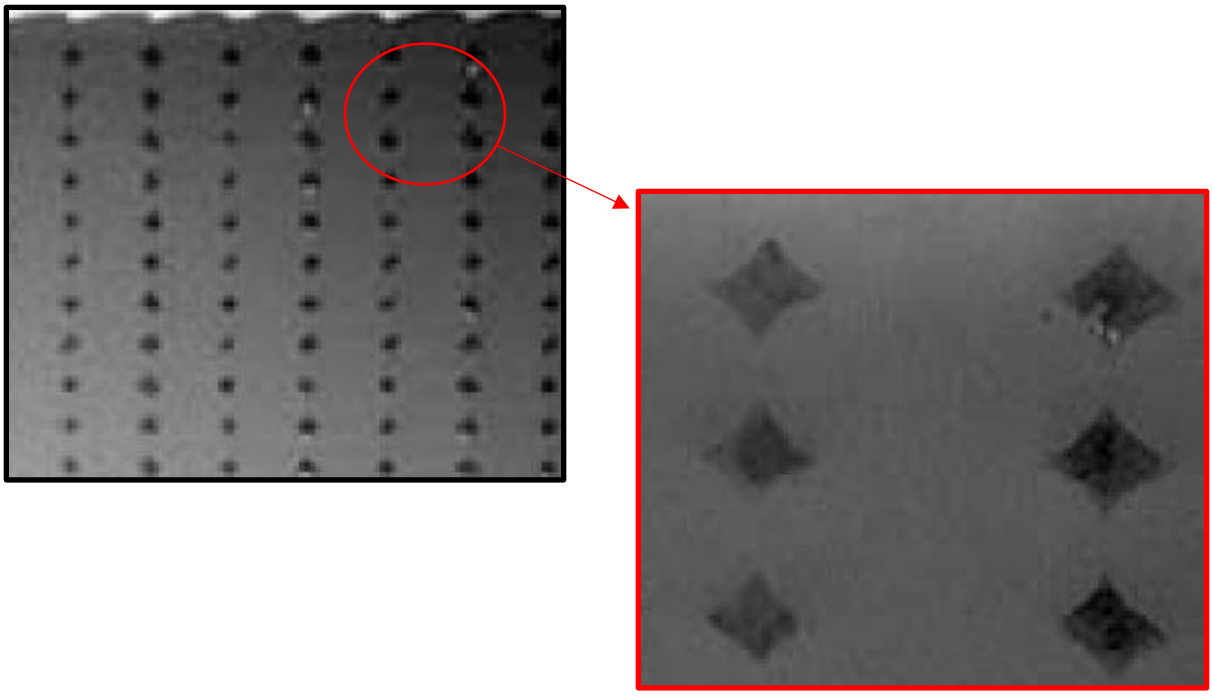

Figure 2- 15: Consistent Negative Gap Results in Better Interfacial Properties

2.18 Conclusion:

In this chapter, non-isothermal numerical simulation results of FDM process were presented. Different parameters affecting temperature history and degree of bonding of filaments were presented and discussed.

It was shown that the diameter of the filaments, the speed at which they print, the temperature of the extruder and the ambient temperature of the FDM machine have significant effect on the degree of bond formation between filaments. Negative gap setting was shown to have a greater effect on the final length of the neck between filaments than the sintering process. Numerical results also confirmed the effect of critical sintering temperature at which the neck's growth rate becomes negligible.

Future research will be conducted on evaluating molecular sintering rate and its effect on the strength development of the interface between filaments.

Chapter 3:

Numerical Modeling of Molecular Diffusion Across the Interface

3.1 Diffusion Model:

Different microscopic theories have been proposed in literature to estimate the degree of molecular diffusion and development of mechanical properties at the interface of amorphous polymers. Pragar and Tirrel[25] proposed a model based on crossing density of polymer chains and deGennes proposed another model based on the number of bridges formed across the polymer interface.

Amorphous polymer diffusion theory used in this research is based on reptation theory proposed by De Gennes in 1971[26]. Reptation is the thermal motion of long entangled molecular chains in polymers above glass transition temperature. Reptation theory assumes polymer chains slithering through each other like snakes. Reptation theory models the motion of individual linear polymer chains in amorphous material and it is widely used to polymer-polymer interface diffusion process under isothermal conditions. It is assumed a polymer chain of length L is confined in a tube, which represents the steric effects of neighborhood chains. Therefore, the chain can only move long its curvilinear length. When the contact between filaments occurs, the polymer chain is confined in the tube, Then the chain moves inside the tube in a Brownian motion manner. After some time, the chain ends form minor chains with other chains that manage to deform out of the original tube shape. At the reptation time, T_R, the entire chain moves out of the original tube boundaries.

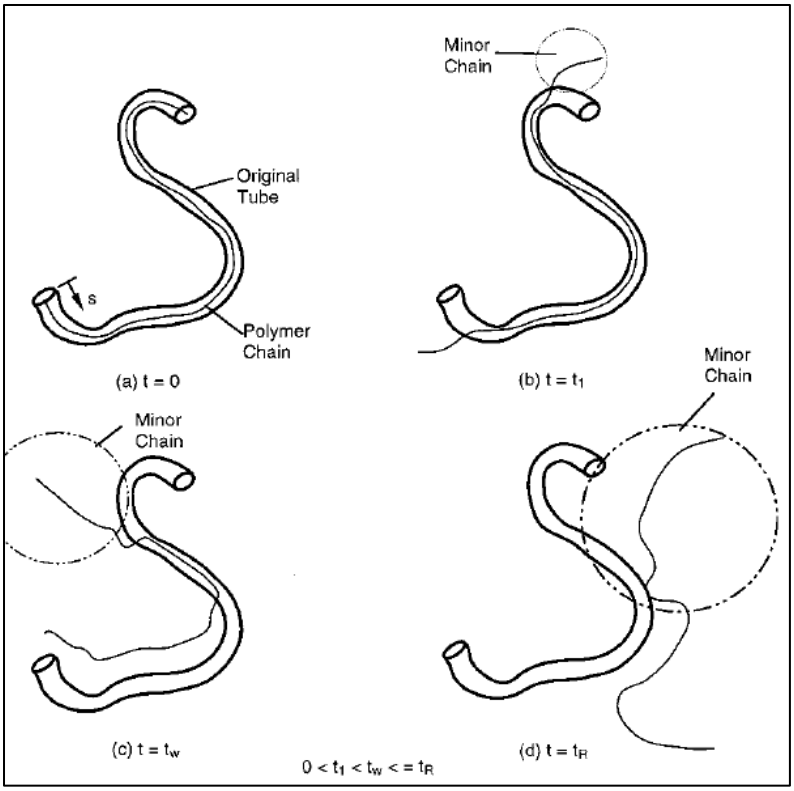

Figure 3- 1: Reptation movement of a linear polymer chain [27]

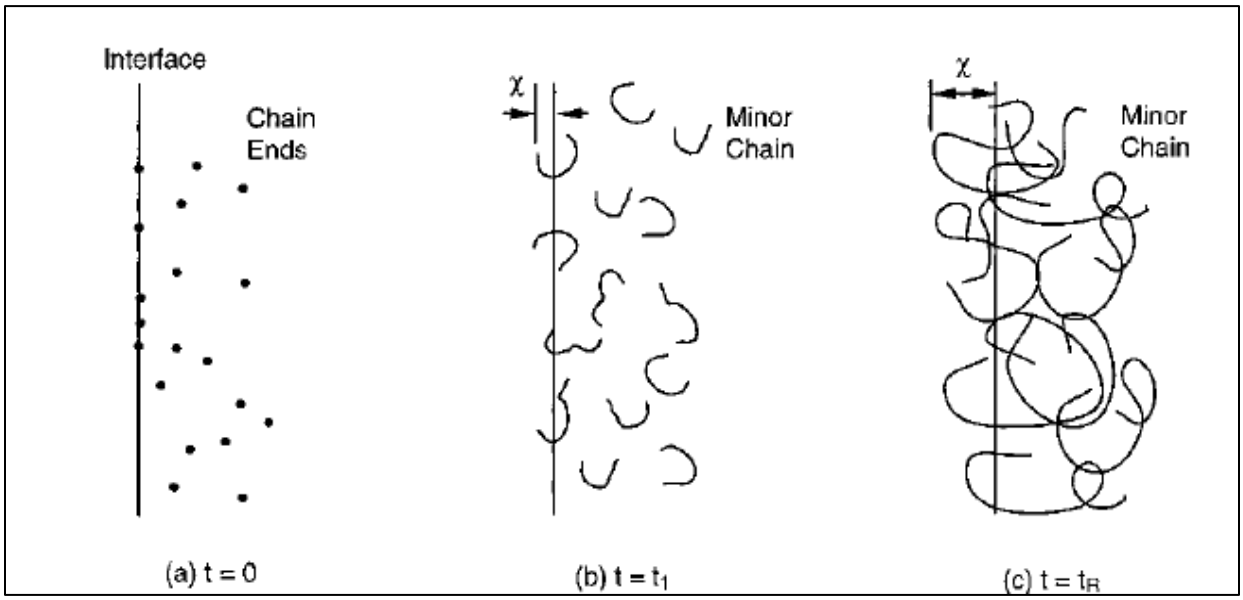

Figure 3- 2: Diffusion of minor chains across a polymer-polymer [27]

chain reptation is the driving force in thermoplastic polymer healing. Polymer healing theory explains the relationship between reptation and development of mechanical properties at the interface of polymers that come in contact at temperatures above glass transition temperature. Most of proposed diffusion theories available in literature are based on isothermal models.

Bastin and Gillespie [28] modified the isothermal reptation theory by approximating the isothermal process to a series of quasi-isothermal processes. In their model, they divided the time domain into a series of time intervals. Each time interval was considered an isothermal process with average temperature of the interval.

$$\frac{\Delta\sigma}{\sigma_\infty} = \frac{{t_{i+1}}^{1/4} + {t_i}^{1/4}}{{t_i}^{1/4}} \tag{3.1}$$

$$D_h(t) = \frac{\sigma}{\sigma_\infty} = \sum_{t=0}^{t/\Delta t} \left\lceil \frac{{t_{i+1}}^{1/4} + {t_i}^{1/4}}{{t_i}^{1/4}} \right\rceil \tag{3.2}$$

Yang [27]in his research questioned the theoretical basis of bastin's model as the series expansion can limit the validity of the diffusion model. Yang and his colleagues used random walk analysis to define a probability density function, P(s,t). The P function defines the probability of polymer chain existence at point s and time t.

Diffusion equation, initial condition and boundary conditions are as follows:

$$\frac{\partial P}{\partial t} = D\ \frac{\partial^2 P}{\partial s^2} \tag{3.3}$$

D represent the reptation diffusion coefficient for back and forth motions of polymer chains. This diffusion coefficient defined base on the molecular weight, temperature and hydrostatic pressure.[29]

$$P(s,0) = \ \delta(0) \tag{3.4}$$

δ is the Dirac delta function.

$$P(s,t) = 0 \tag{3.5}$$

$$\frac{\partial P(s,t)}{\partial t} = 0\ \ as\ |s| \rightarrow\ \infty \tag{3.6}$$

under isothermal condition D0 is constant then the solution becomes the below probability density function[25]:

$$P(s,t) = \ \frac{1}{[4\pi D_0 t]^{\frac{1}{2}}}\ e^{\left[{-s^2}/{4D_0\, t}\right]} \tag{3.7}$$

$$< s^2 >= \ \int_{-\infty}^{+\infty} s^2 P(s,t)\ ds = 2D_0 t \tag{3.8}$$

Welding time is defined as:

$$t_w(T_0) = \ \frac{{L_W}^2}{2D_0} \tag{3.9}$$

L_W is minor chain length

A Fourier Transformation of equation 3.3, with its boundary conditions, equation 3.4 and 3.5. Results as follows:

$$\frac{\partial P}{\partial t} = -D(t)\omega^2 P \tag{3.10}$$

ω is the transformed variable in the frequency domain and P is the Fourier transformation of the probability density function.

$$P(\omega, t) = \frac{1}{\sqrt{2\pi}} \int_{-\infty}^{+\infty} P(s, t) \exp(-i\omega s)\, ds \tag{3.11}$$

$$P(\omega, 0) = \frac{1}{\sqrt{2\pi}} \tag{3.12}$$

Now inverse Fourier transformation of solution:

$$P(s, t) = \frac{1}{\sqrt{2\pi}} \int_{-\infty}^{+\infty} P(\omega, t) \exp(i\omega s)\, d\omega \tag{3.13}$$

$$= \frac{1}{2\pi} \int_{-\infty}^{+\infty} \exp\left[\omega^2 \int_0^t -D(t)dt\right] \cos(\omega s)\, d\omega$$

From above equations it can be derived:

$$D_h(t) = \frac{K}{K_\infty} = \frac{\sigma}{\sigma_\infty} = \left(\frac{1}{L_w}\right)^{1/2} = \left[\int_0^t \frac{1}{t_w(T)} dt\right]^{1/4} \tag{3.14}$$

K is fracture toughness, K_∞ is fracture toughness of the fully healed filaments, σ is ultimate strength, σ_∞ is the ultimate strength of the fully healed filaments and t_w is diffusion time as a function of temperature.

Diffusion time then defined as an Arrhenius relationship with temperature as follows:[30]

$$t_w = A.exp\left(\frac{E}{R}\left(\frac{1}{T} - \frac{1}{T_{ref}}\right)\right) \tag{3.15}$$

Where A is 4624 s, E is 10^5 kJ/kmol, R is the universal gas constant 8.314 (KJ/mol.K) and T_{ref} is 643 K.

3.2 Estimate of Interfacial Material Properties:

As equation 3.14 indicates, development of the interfacial mechanical properties between adjacent filaments is a function of diffusion time. And the diffusion time is a function of filaments temperature. Considering that the FDM process is a transient thermal process and filaments lose thermal energy rapidly, in most cases the diffusion time is not long enough for the material properties to fully develop; Therefore, the final interfacial material properties such as fracture toughness and ultimate strength differ from the bulk material properties. The below equations are used to estimate the final interfacial mechanical properties developed between filaments:

$$\lim_{t\to\infty} K_\infty D_h(t) = K \tag{3.16}$$

$$\lim_{t\to\infty} \sigma_\infty D_h(t) = \sigma \tag{3.17}$$

3.3 Results and Discussions:

As shown in the following figures, the degree of molecular diffusion and development of mechanical properties at the interface is directly dependent on the area under the temperature curve. Therefore, by increasing heat capacity of the filaments and initial diffusion temperature at the interface higher mechanical properties can be achieved.

The effect of negative gap is also very important. As with higher negative gap setting, more molecules at the interface experience the highest thermal energy of initial diffusion temperature. The molecules that come in contact later due to the sintering process do not play an important role to the development of mechanical properties of the interface as they experience lower initial diffusion temperature and their temperature stays above the glass transition temperature for a shorter amount of time.

3.4 Filament Diameter:

Increasing filament diameter from 0.3mm to 0.6mm results in 42% improvement in interfacial mechanical properties. This signifies the importance of the higher initial diffusion temperature due to the higher heat capacity of larger filaments.

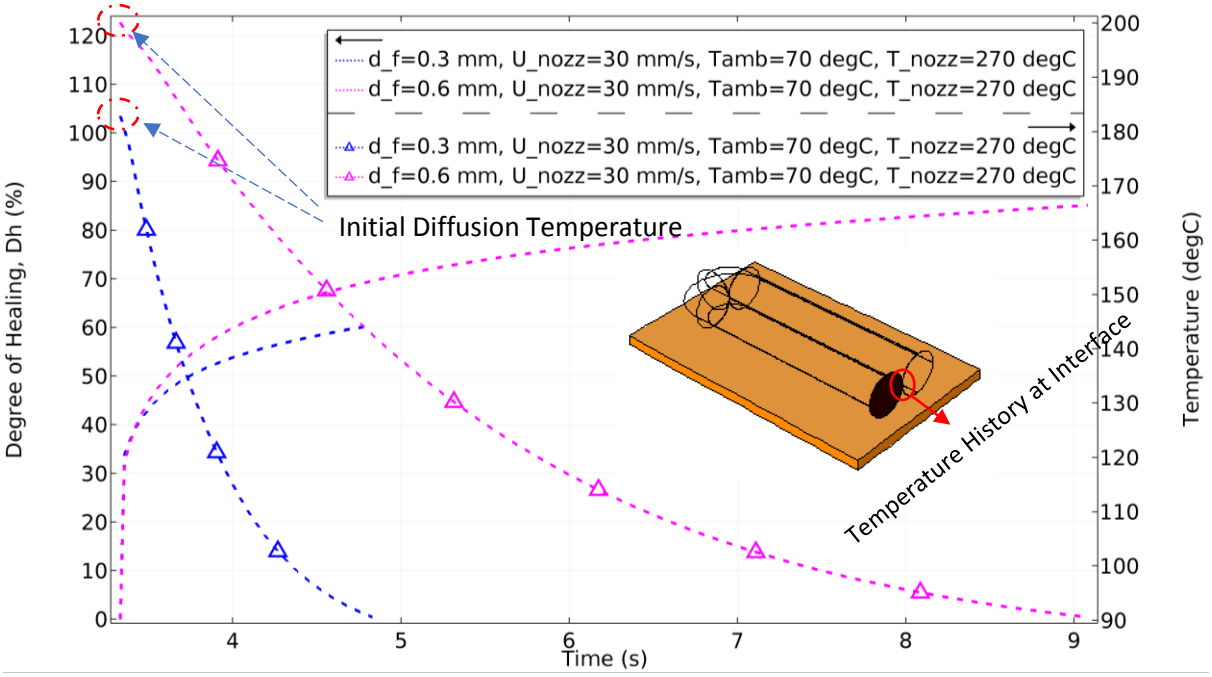

Figure 3- 3: Temperature History and Diffusion Rate at Interface for Different Filament Diameters

3.5 Print Speed (Nozzle Speed):

An Increase in print speed from 30 mm/s to 200 mm/s results in higher diffusion rate between filaments. This increase in diffusion rate due to higher print speed is more significant for higher diameter filaments as shown in Figures 3-4 and 3-5. For 0.3mm diameter filaments the print speed increase results in 5% improvement in diffusion rate and for 0.6 mm diameter filaments a 10% improvement was achieved.

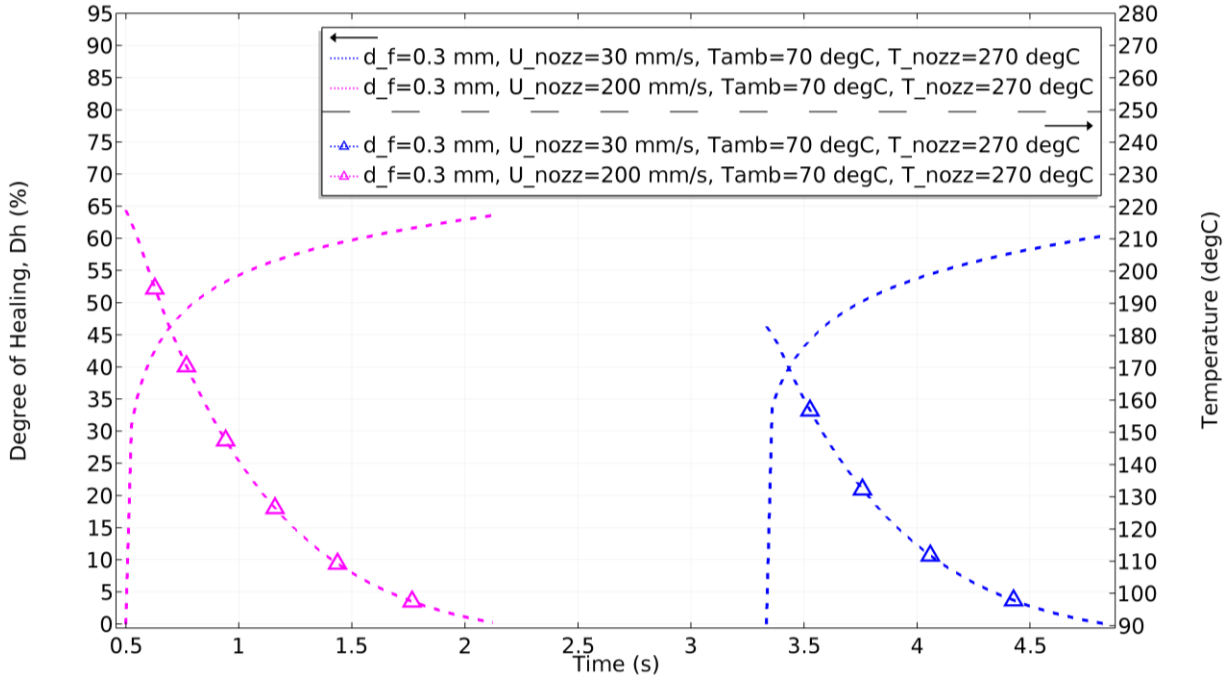

Figure 3- 4: Temperature History and Diffusion Rate for 0.3 mm Filaments

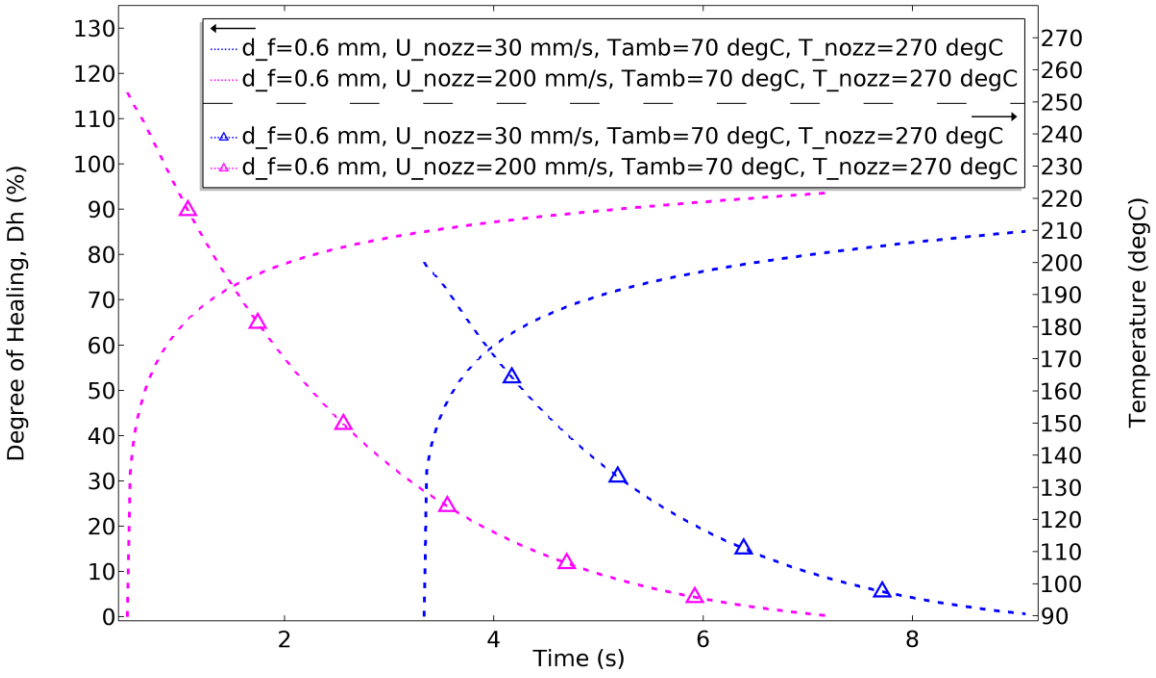

Figure 3- 5:Temperature History and Diffusion Rate for 0.6 mm Filaments

3.6 Extrusion temperature:

Extrusion temperature increase from 220 ºC to 270 ºC results in 8% improvement in mechanical properties.

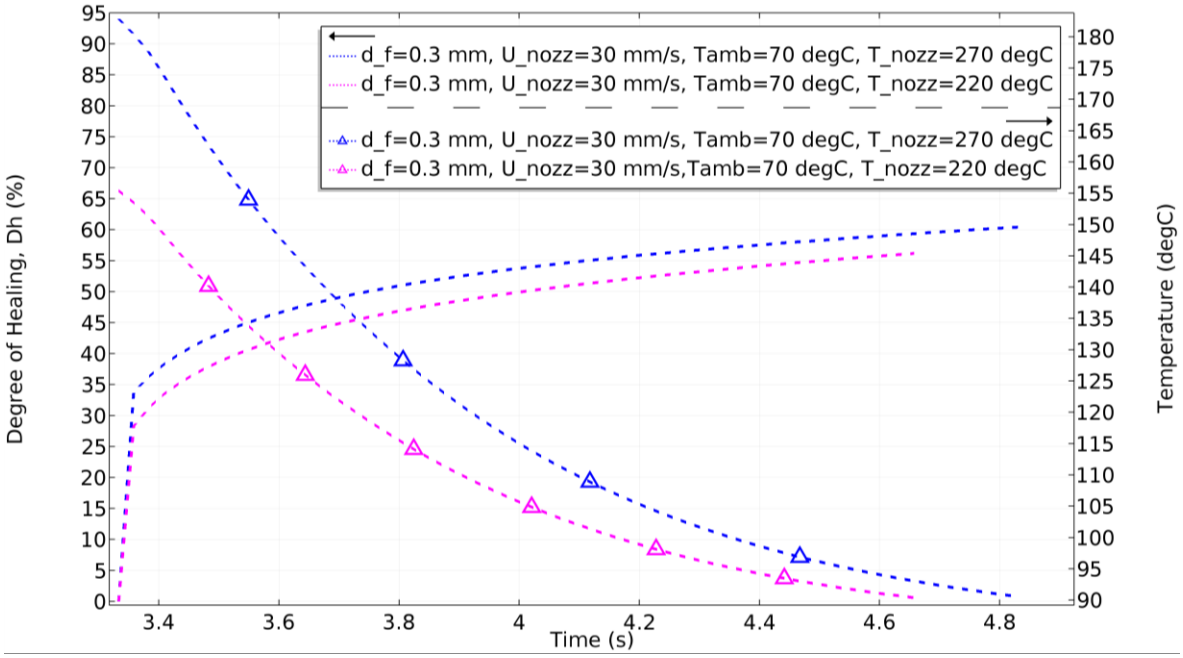

Figure 3- 6: Temperature History and Diffusion Rate at Interface for Different Extrusion Temperatures

3.7 Envelope temperature:

Envelope temperature increase has a minor effect on the initial diffusion temperature and as shown in Figure3-6, a change in the envelope temperature from 50 ºC to 70 ºC results in 2% improvement in mechanical properties.

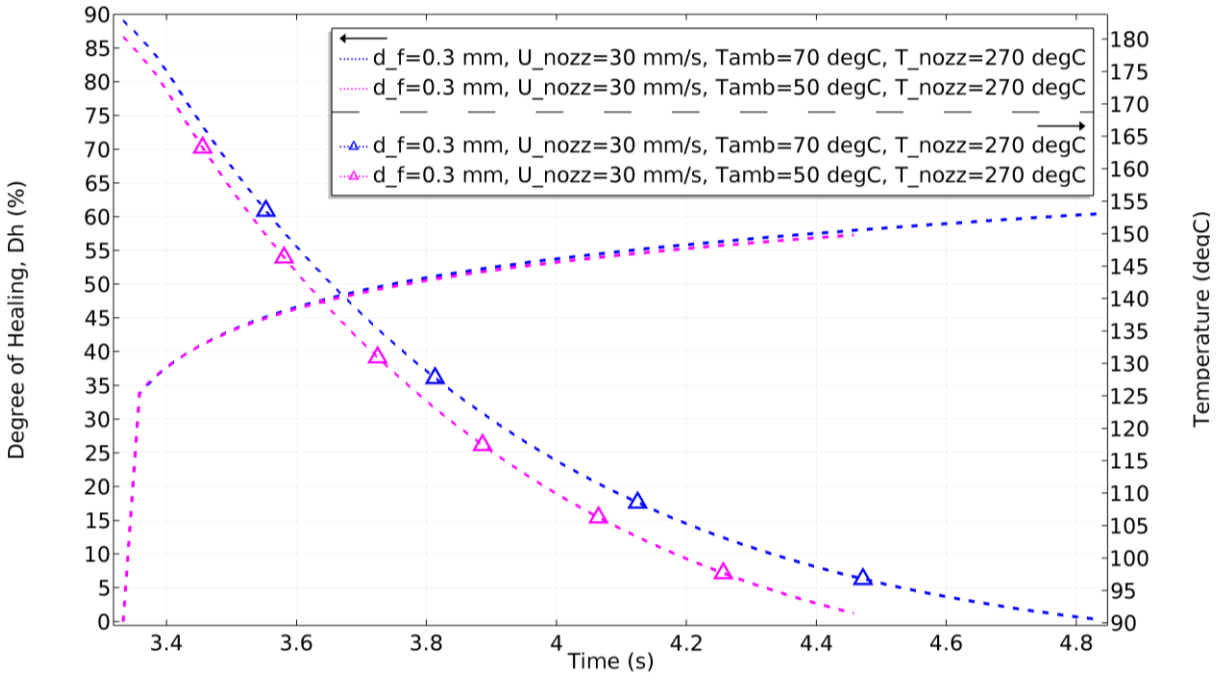

Figure 3- 7: Temperature History and Diffusion Rate at Interface for Different Envelope Temperature

3.8 Gap Setting:

Increase in gap setting does not affect the diffusion rate of the molecules at the interface, However, by increasing the negative gap setting, the interface between filaments increases. Hence more molecules experience the initial diffusion temperature at the interface: therefore, stronger mechanical properties are developed.

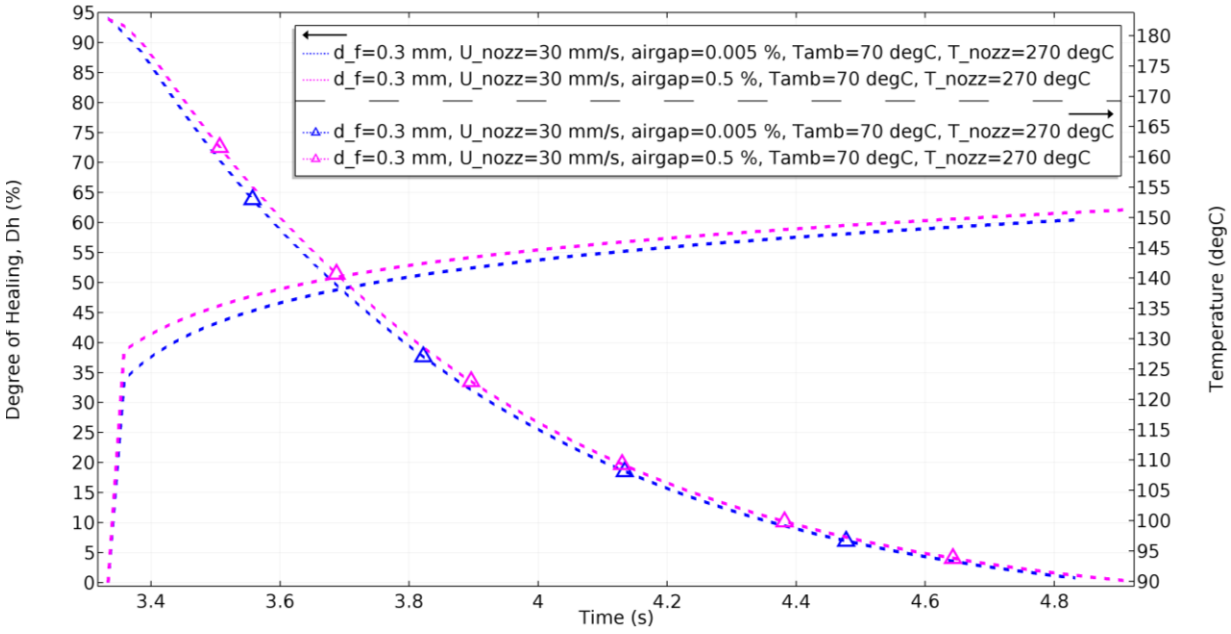

Figure 3- 8: Temperature History and Diffusion Rate at Interface for Different Gap Settings

3.9 Conclusion:

In this chapter, non-isothermal molecular diffusion results of FDM process were presented. Different parameters affecting the molecular diffusion rate and development of mechanical properties of the interface were presented and discussed.

It was shown that the rate of development of mechanical properties at the interface is directly dependent on the area under the interface temperature curve and specifically related to the initial diffusion temperature. Increase in the diameter of the filaments significantly improve the interfacial mechanical properties of the filaments.

Negative gap setting was shown to have a negligible effect on the molecular diffusion rate at the interface; However, higher negative gap setting increases the interface length and more molecules at the interface experience the high initial diffusion temperature, Therefore, Higher mechanical properties are developed.

The effect of sintering process in the development of the mechanical properties at the interface was determined to be negligible since the molecules that come in contact due to the sintering process stay above the glass transition temperature for a very short amount of time compared to the molecules that come in contact at the initial diffusion time and thy do not experience the high initial diffusion temperature which is responsible for the highest diffusion rate between molecules.

The results of this research indicate that there needs to be a diffusion coefficient to be used for determination of interfacial material properties of filaments.

Future research will be conducted on development of more accurate Arrhenius equation for ABS polymer and development of nozzle cross sections to increase the initial diffusion length of interface.

Chapter 4:

Fracture Mechanics Study of Stress Singularity Points in FDM Parts

4.1 Fracture Mechanics Model:

The deformed meshes obtained from non-isothermal polymer sintering models show that the interface healing occurs partially between adjacent filaments. This partial healing results in creation of singularity points at the interface. The singularity points at the interface result in singular stress field at the vicinity of the singular point. The effects of these singularity points are assessed with fracture mechanics principals.

The singularity points resemble to sharp V-notch corners with different opening angles depending on the gap setting (Distance between the center of the filaments). The healing interface with two singularities can be modeled as a Double Edge Notched Tension (DENT) model with plain strain condition.

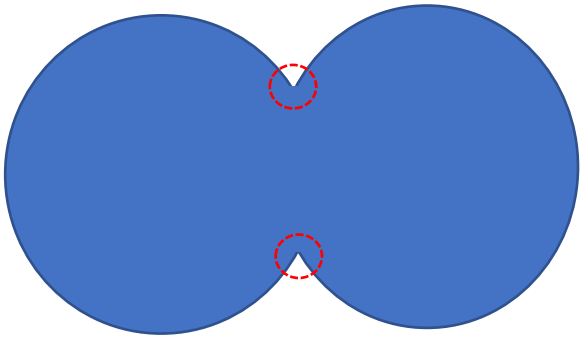

Figure 4- 1: Locations of Singularity Points

4.2 Stress Intensity Factor:

Stress intensity factor is used to predict the state and magnitude of the stress near the crack or slit tips.

Linear Elastic Fracture Mechanics (LEFM) is a typical fracture behavior for polymers below the glass transition temperature [31] ; therefore, LEFM is used in this research for study of the inter-filament fractures of FDM parts.

Figure 4-2 shows the state of stresses near the crack tip for elastic materials for mode I fracture. K_1, is a constant known as stress intensity factor, that defines the stress distribution at the tip of the crack for linear elastic materials.

It should be noted that the SIF for notches exist between adjacent filaments has different characteristics since the state of stress field at notch singularity is different from the crack stress fiend.

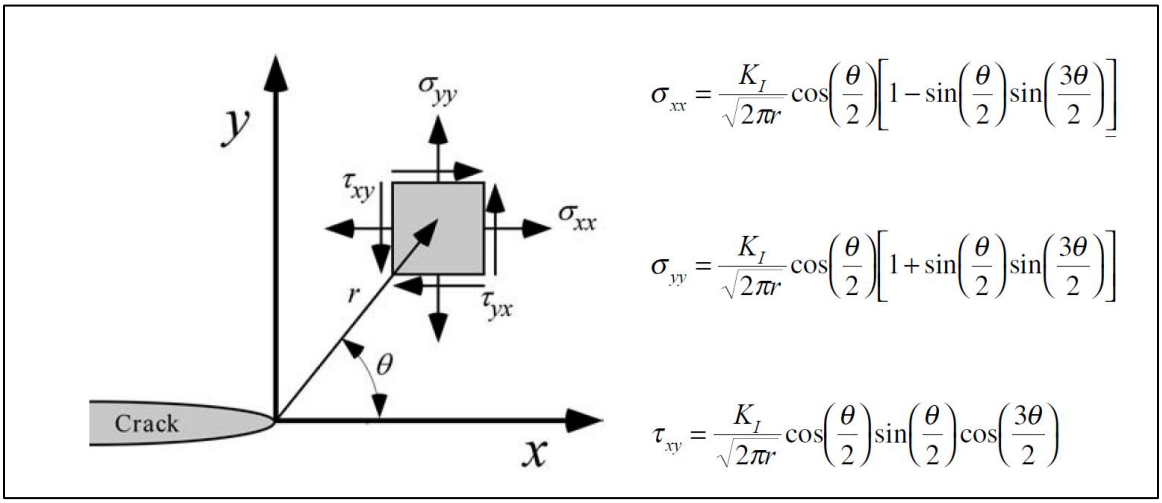

Figure 4- 2: State of Stresses Near the Hairline Crack Tip

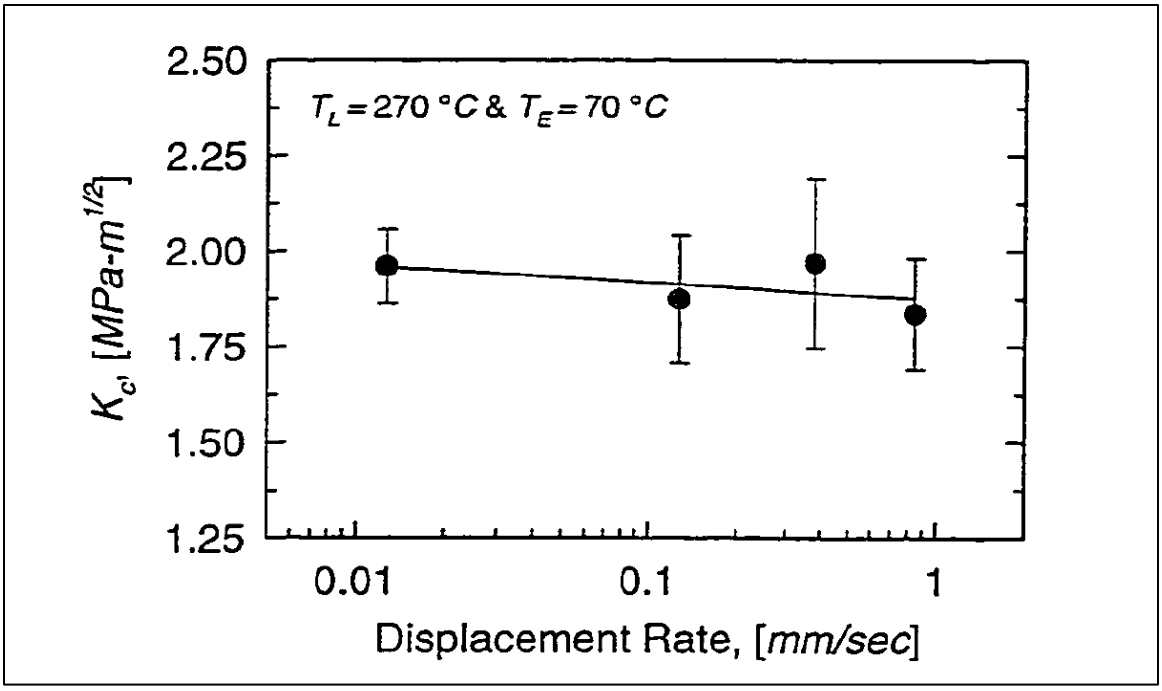

Figure 4- 3: Interfacial Fracture Toughness for ABS Filaments [3]

4.3 Eigenfunction Series Expansion Method for Notch Stress Intensity:

In Figure 4-2, stress equations near the crack tip has been illustrated. In the near field stress equations, the equations have an inverse square root of r, which is called singularity order for the crack tip. In addition, the near field stress functions do not depend on the applied loads and the geometry of the cracked specimen. Eigenfunction expansion method introduced by Williams [32, 33] is a general form that can be used for any crack geometry and loading condition.

Since the angle of the singularity points, notch angle between filaments, changes with change in filament diameter and gap setting the Eigenfunction Series Expansion Method was used to study Notch Singularity Factor, NSIF, for extruded filaments.

In two-dimensional formulation of stress field at the sharp vertex of a notch in linear elastic materials, stress and strains equations are known to have singularity order of $r^{\lambda-1}$, where λ is dependent on the angle of the notch.

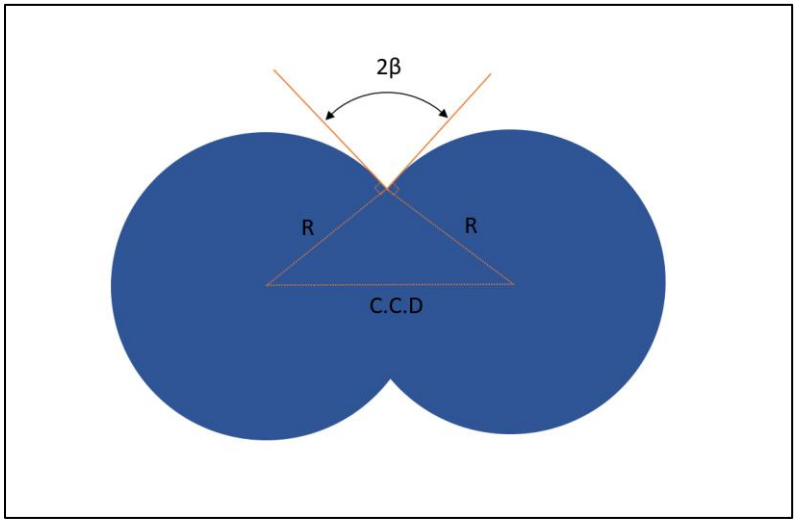

Figure 4- 4: Angle at the Vertex of the Notch

Notch angle between two filaments is defined per:

$$2\beta = \cos^{-1}\left(\frac{(d_f - d_f\frac{gp}{100})^2 - 2r^2}{2r^2}\right) \quad (4.1)$$

Where r is radius of the filament and d_f is diameter of the filament and gp is the negative gap percentage (%) value.

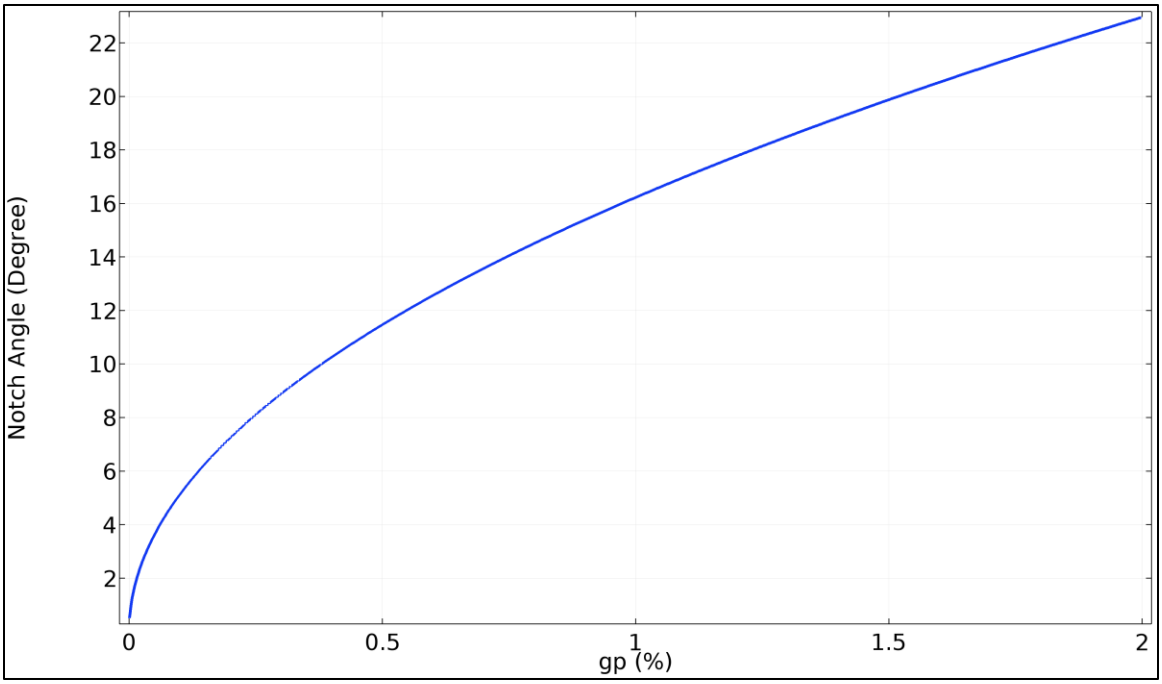

Figure 4- 5: Notch Angle (2β) VS Negative Gap setting

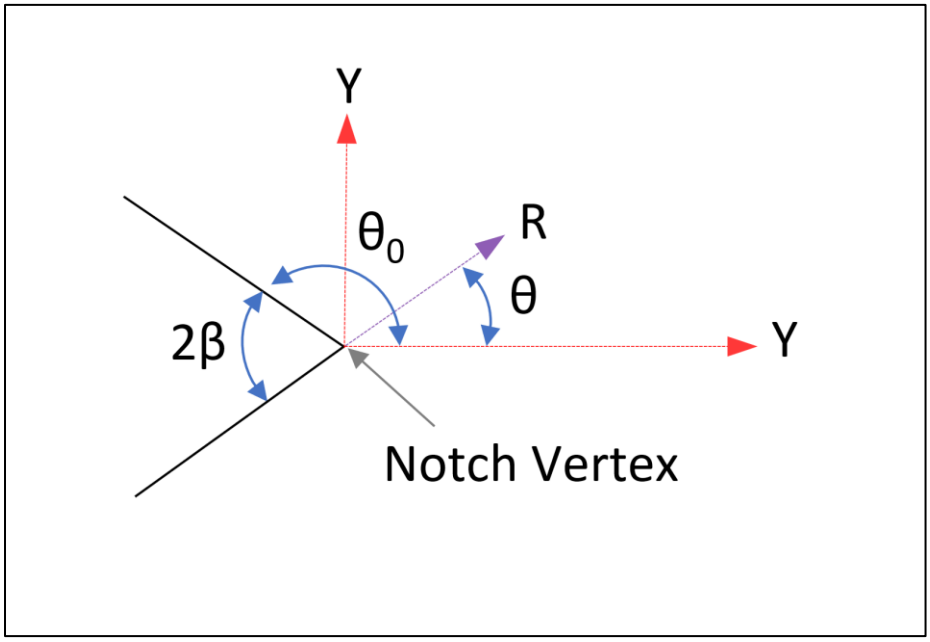

Figure 4- 6: Sharp Notch with 2β Angle in Polar Coordinate System

Equations of equilibrium in polar coordinate system are:

$$\frac{\partial \sigma_{rr}}{\partial r} + \frac{1}{r}\frac{\partial \sigma_{r\theta}}{\partial \theta} + \frac{\sigma_{rr} - \sigma_{\theta\theta}}{r} = 0 \tag{4.2}$$

$$\frac{\partial \sigma_{r\theta}}{\partial r} + \frac{1}{r}\frac{\partial \sigma_{\theta\theta}}{\partial \theta} + 2\frac{\sigma_{r\theta}}{r} = 0 \tag{4.3}$$

Airy Stress Function is used to satisfy the above equilibrium equations

$$\sigma_{rr} = \frac{1}{r^2}\frac{\partial^2 \phi}{\partial \theta^2} + \frac{1}{r}\frac{\partial \phi}{\partial r} \tag{4.4}$$

$$\sigma_{\theta\theta} = \frac{\partial^2 \phi}{\partial r^2} \tag{4.5}$$

$$\sigma_{r\theta} = \frac{1}{r^2}\frac{\partial \phi}{\partial \theta} - \frac{1}{r}\frac{\partial^2 \phi}{\partial r \partial \theta} = -\frac{\partial}{\partial r}\left(\frac{1}{r}\frac{\partial \phi}{\partial \theta}\right) \tag{4.6}$$

And Strains using are as follows:

$$\varepsilon_{rr} = \frac{\partial u_r}{\partial r} \tag{4.7}$$

$$\varepsilon_{\theta\theta} = \frac{u_r}{r} + \frac{1}{r}\frac{\partial u_\theta}{\partial \theta} \tag{4.8}$$

$$\gamma_{r\theta} = \frac{1}{r}\frac{\partial u_r}{\partial \theta} + \frac{\partial u_\theta}{\partial r} - \frac{u_\theta}{r} \tag{4.9}$$

For plain strain condition, stress and strain relationships per hooks law are:

$$\varepsilon_{rr} = \frac{1+\nu}{E}[(1-\nu)\sigma_{rr} - \nu\sigma_{\theta\theta}] \tag{4.10}$$

$$\varepsilon_{\theta\theta} = \frac{1+\nu}{E}[-\nu\sigma_{rr} - (1-\nu)\sigma_{rr}] \tag{4.11}$$

$$\varepsilon_{r\theta} = \frac{1+\nu}{E}\sigma_{r\theta} \tag{4.12}$$

Compatibility equation for polar coordinates is defined as:

$$\frac{1}{r^2}\frac{\partial^2 \varepsilon_{rr}}{\partial \theta^2} + \frac{\partial^2 \varepsilon_{\theta\theta}}{\partial r^2} - \frac{2}{r}\frac{\partial^2 \varepsilon_{r\theta}}{\partial r \partial \theta} - \frac{1}{r}\frac{\partial \varepsilon_{rr}}{\partial r} + \frac{2}{r}\frac{\partial \varepsilon_{\theta\theta}}{\partial r} - \frac{2}{r^2}\frac{\partial \varepsilon_{r\theta}}{\partial \theta} = 0 \tag{4.13}$$

From the compatibility equation and the equilibrium equation Airy Stress Function is defined.

$$\nabla^2 \nabla^2 \phi = 0 \tag{4.14}$$

$$\nabla^2 = \frac{\partial^2}{\partial r^2} + \frac{1}{r}\frac{\partial}{\partial r} + \frac{1}{r^2}\frac{\partial^2}{\partial \theta^2} \tag{4.15}$$

Solving a fourth order partial differential equation using a separation of variable technique:

$$\phi\,(r,\theta) = r^{\lambda_n+1} F_n(\theta) \tag{4.16}$$

Then the airy stress function can be expanded into the following series:

$$\phi\,(r,\theta) = \sum_{n=0}^{\infty} r^{\lambda_n+1} F_n(\theta) \tag{4.17}$$

λ_n is Eigenvalues and $F_n(\theta)$is the corresponding Eigen Functions.

Now Eq 4.17 is substituted in Eq 4.14

$$\frac{d^4 F_n(\theta)}{d\theta^4} + 2\left(\lambda_n{}^2 + 1\right)\frac{d^2 F_n(\theta)}{d\theta^2} + \left(\lambda_n{}^2 - 1\right)^2 F_n(\theta) = 0 \tag{4.18}$$

the solution for $F_n(\theta)$ in eq 4.18:

$$F_n(\theta) = A_n \sin((\lambda_n + 1)\,\theta) + B_n \cos((\lambda_n + 1)\,\theta) + C_n \sin((\lambda_n - 1)\,\theta) + D_n \cos((\lambda_n - 1)\,\theta) \tag{4.19}$$

$A_n, B_n, C_n, D_n$are unknown constants.

The unknown constants with the eigenvalue have to be found using the free boundary condition along the crack surfaces: (for $\theta = \pm\theta_0 = \pi + \beta$ & $\beta - \pi$)

$$\sigma_{\theta\theta} = 0 \tag{4.20}$$

$$\sigma_{r\theta} = 0 \tag{4.21}$$

Since the Airy stress function should be an even function of θ (for mode one NSIF,KI). The constant for Sinus terms become zero.

$$\phi\,(r,\theta) = \sum_{n=0}^{\infty} r^{\lambda_n+1}[B_n \cos((\lambda_n+1)\,\theta) + D_n \cos((\lambda_n-1)\,\theta)] \tag{4.22}$$

Now stresses in the polar coordinate system are:

$$\sigma_{rr} = \frac{1}{r^2}\frac{\partial^2\phi}{\partial\theta^2} + \frac{1}{r}\frac{\partial\phi}{\partial r} = \sum_{n=0}^{\infty} r^{\lambda_n-1}[F_n{}''(\theta) + (\lambda_n+1)F_n(\theta)] \tag{4.23}$$

Therefore:

$$\sigma_{rr} = -\sum_{n=0}^{\infty} \lambda_n r^{\lambda_n-1}[B_n(\lambda_n+1)\cos((\lambda_n+1)\,\theta) + D_n(\lambda_n-3)\cos((\lambda_n-1)\,\theta)] \tag{4.24}$$

$$\sigma_{\theta\theta} = \frac{\partial^2\phi}{\partial r^2} = \sum_{n=0}^{\infty} r^{\lambda_n-1}\lambda_n(\lambda_n+1)F_n(\theta) \tag{4.25}$$

$$\sigma_{\theta\theta} = \sum_{n=0}^{\infty} r^{\lambda_n-1}\lambda_n(\lambda_n+1)[B_n \cos((\lambda_n+1)\,\theta) + D_n \cos((\lambda_n-1)\,\theta)] \tag{4.26}$$

$$\sigma_{r\theta} = -\frac{\partial}{\partial r}\left(\frac{1}{r}\frac{\partial\phi}{\partial\theta}\right) = -\sum_{n=0}^{\infty} \lambda_n r^{\lambda_n-1}F_n{}'(\theta) \tag{4.27}$$

$$\sigma_{r\theta} = \sum_{n=0}^{\infty} \lambda_n r^{\lambda_n - 1}[B_n(\lambda_n + 1)\sin((\lambda_n + 1)\,\theta) + D_n(\lambda_n - 1)\sin((\lambda_n - 1)\,\theta)] \tag{4.28}$$

Now using hooks law, Strains are:

$$\frac{\partial u_r}{\partial r} = \frac{1}{2G}\left[\sigma_{rr} - \frac{3-\kappa}{4}(\sigma_{rr} + \sigma_{\theta\theta})\right] \tag{4.29}$$

$$\frac{u_r}{r} + \frac{1}{r}\frac{\partial u_\theta}{\partial \theta} = \frac{1}{2G}\left[\sigma_{\theta\theta} - \frac{3-\kappa}{4}(\sigma_{rr} + \sigma_{\theta\theta})\right] \tag{4.30}$$

$$\frac{1}{r}\frac{\partial u_r}{\partial \theta} + r\frac{\partial}{\partial r}\left(\frac{u_\theta}{r}\right) = \frac{1}{2G}\sigma_{r\theta} \tag{4.31}$$

For plane strain

$$\kappa = 3 - 4\nu \tag{4.32}$$

Now from the above equations we can derive:

$$u_r = \frac{1}{2G}\sum_{n=0}^{\infty} r^{\lambda_n}[-(\lambda_n + 1)F_n(\theta) + (1+\kappa)D_n\cos((\lambda_n - 1)\,\theta)] \tag{4.33}$$

$$u_\theta = \frac{1}{2G}\sum_{n=0}^{\infty} r^{\lambda_n}[-F_n{}'(\theta) + (1+\kappa)D_n\sin((\lambda_n - 1)\,\theta)] \tag{4.34}$$

Where G is the shear modulus and ν is the Poisson's ratio.

Using boundary condition

$$B_n\,(\lambda_n + 1)\sin((\lambda_n + 1)\,\theta_0) + D_n\,(\lambda_n - 1)\cos((\lambda_n - 1)\,\theta_0) = 0 \tag{4.35}$$

$$B_n\cos((\lambda_n + 1)\,\theta_0) + D_n\cos((\lambda_n - 1)\,\theta_0) = 0 \tag{4.36}$$

In order for these equations to have nontrivial solutions the determinant of the coefficients must be zero; Therefore, the characteristic equation for λ_n becomes:

$$\lambda_n\sin(2\theta_0) + \sin(2\lambda_n\theta_0) = 0 \tag{4.37}$$

Then the ratio between B_n & D_n is:

$$B_n = -\frac{(\lambda_n - 1)\sin\big((\lambda_n - 1)\theta_0\big)}{(\lambda_n + 1)\sin\big((\lambda_n + 1)\theta_0\big)} D_n \tag{4.38}$$

Now with $\lambda_n$being the nth root of the equation 4.40. the symmetric solution for airy function is:

$$\phi\,(r,\theta) = \sum_{n=0}^{\infty} D_n r^{\lambda_n+1}\left[-\frac{(\lambda_n - 1)\sin\big((\lambda_n - 1)\theta_0\big)}{(\lambda_n + 1)\sin\big((\lambda_n + 1)\theta_0\big)}\cos((\lambda_n + 1)\,\theta) + \cos((\lambda_n - 1)\,\theta)\right] \tag{4.39}$$

Then the stress equations become

$$\sigma_{rr} = \sum_{n=1}^{\infty} D_n \lambda_n r^{\lambda_n - 1}\left[(3 - \lambda_n)\cos((\lambda_n - 1)\theta) + \frac{(\lambda_n - 1)\sin\big((\lambda_n - 1)\theta_0\big)}{\sin\big((\lambda_n + 1)\theta_0\big)}\cos((\lambda_n + 1)\,\theta)\right] \tag{4.40}$$

$$\sigma_{\theta\theta} = \sum_{n=0}^{\infty} D_n r^{\lambda_n - 1}\lambda_n(\lambda_n + 1)\left[\cos((\lambda_n - 1)\,\theta) - \frac{(\lambda_n - 1)\sin\big((\lambda_n - 1)\theta_0\big)}{(\lambda_n + 1)\sin\big((\lambda_n + 1)\theta_0\big)}\cos((\lambda_n + 1)\,\theta)\right] \tag{4.41}$$

$$\sigma_{r\theta} = \sum_{n=0}^{\infty} D_n \lambda_n r^{\lambda_n - 1}\left[-\frac{(\lambda_n - 1)\sin\big((\lambda_n - 1)\theta_0\big)}{\sin\big((\lambda_n + 1)\theta_0\big)}\sin((\lambda_n + 1)\,\theta) + (\lambda_n - 1)\sin((\lambda_n - 1)\,\theta)\right] \tag{4.42}$$

From the characteristic equation 4.37 all possible values of λ_n are obtained.

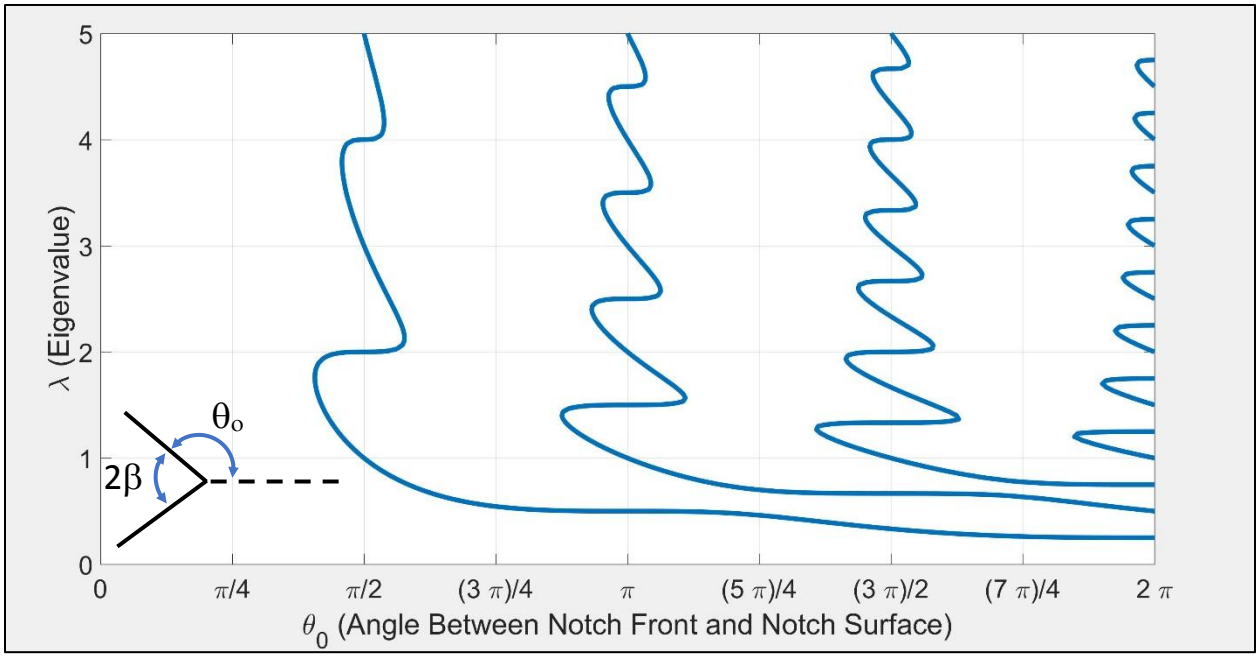

Figure 4- 7: Eigenvalue λ versus θ₀

For a case of hairline crack with $\theta_0 = \pm 180^0$ from equation 4.37:

$$\sin(2\pi\lambda_n) = 0 \tag{4.43}$$

The roots then are

$$\lambda_n = \frac{n}{2} \; with \; n = \pm 1, \pm 2, \ldots\ldots \tag{4.44}$$

With the smallest positive root of $\lambda_n = 1/2$ the inverse square root singularity at the crack tip appears in the equation.

By numerically solving the characteristic equation the only singular term the stress field equations are the following terms:

(4.45)

$$\sigma_{rr} = \frac{K_1}{(2\pi r)^{1-\lambda}}\lambda_n\left[(3-\lambda_n)\cos((\lambda_n-1)\theta) + \frac{(\lambda_n-1)\sin\big((\lambda_n-1)\theta_0\big)}{\sin\big((\lambda_n+1)\theta_0\big)}\cos((\lambda_n+1)\,\theta)\right]$$

(4.46)

$$\sigma_{\theta\theta} = \frac{K_1}{(2\pi r)^{1-\lambda}}\lambda_n(\lambda_n+1)\left[\cos((\lambda_n-1)\,\theta) - \frac{(\lambda_n-1)\sin\big((\lambda_n-1)\theta_0\big)}{(\lambda_n+1)\sin\big((\lambda_n+1)\theta_0\big)}\cos((\lambda_n+1)\,\theta)\right]$$

(4.47)

$$\sigma_{r\theta} = \frac{K_1}{(2\pi r)^{1-\lambda}}\lambda_n\left[-\frac{(\lambda_n-1)\sin\big((\lambda_n-1)\theta_0\big)}{\sin\big((\lambda_n+1)\theta_0\big)}\sin((\lambda_n+1)\,\theta) + (\lambda_n-1)\sin((\lambda_n-1)\,\theta)\right]$$

Then Stress intensity factor

$$K_1 = \lim_{\theta=0\,,r\to 0}\left[(2\pi r)^{1-\lambda}\sigma_{\theta\theta}(r,\theta)\right] \tag{4.48}$$

The practical values of θ_0 is $90 < \theta_0 < 180$ and for λ is $\lambda < 1$. For values of $\lambda > 1$ the stress field is not singular. Figure 4-8 zooms in practical section of Figure 4-7 with valid physical meaning.

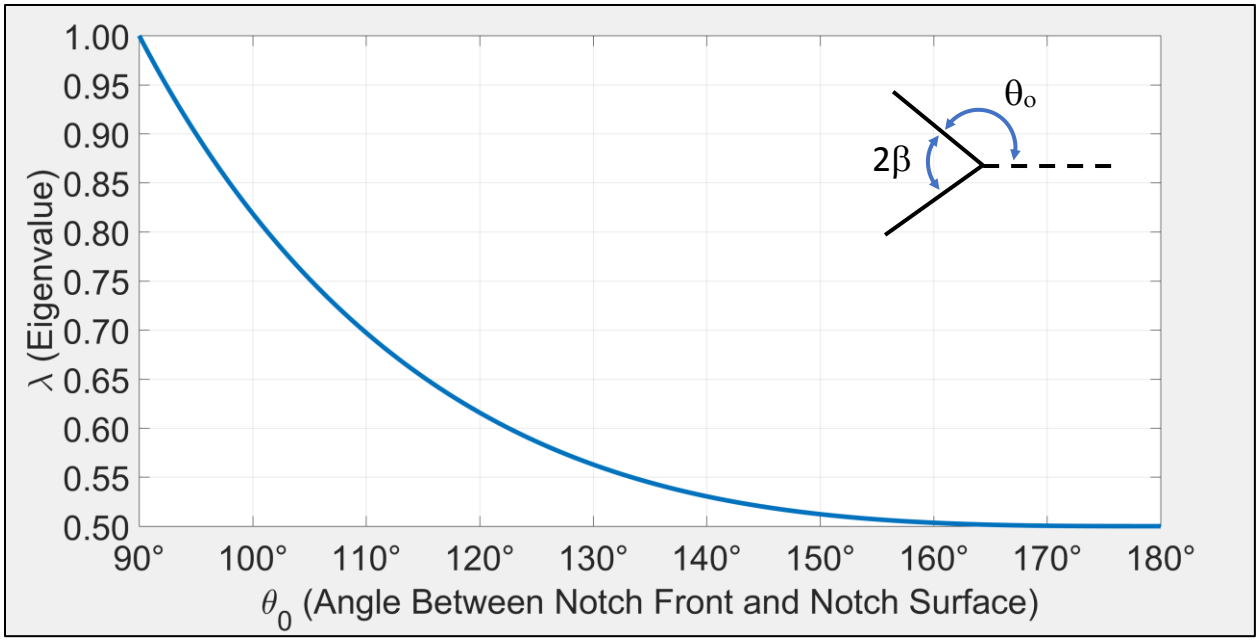

Figure 4- 8: Practical solution range for characteristic function

As discussed in chapter 2, there is a limit to negative airgap setting for 3D printers. Higher negative airgap setting results in jamming the printer nozzle and poor print quality. Conventional negative gap setting and resulting notch angles for FDM parts are illustrated in Figure 4-9.

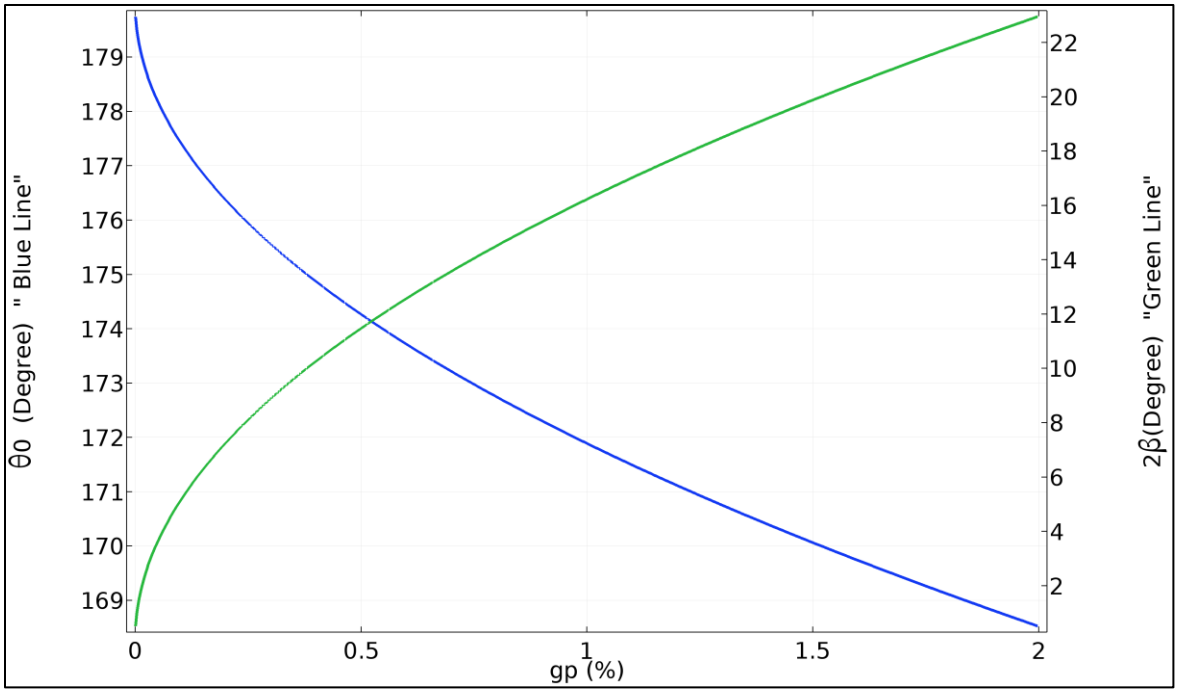

Figure 4- 9: β & θ_0 Values for Different Negative Gap Setting

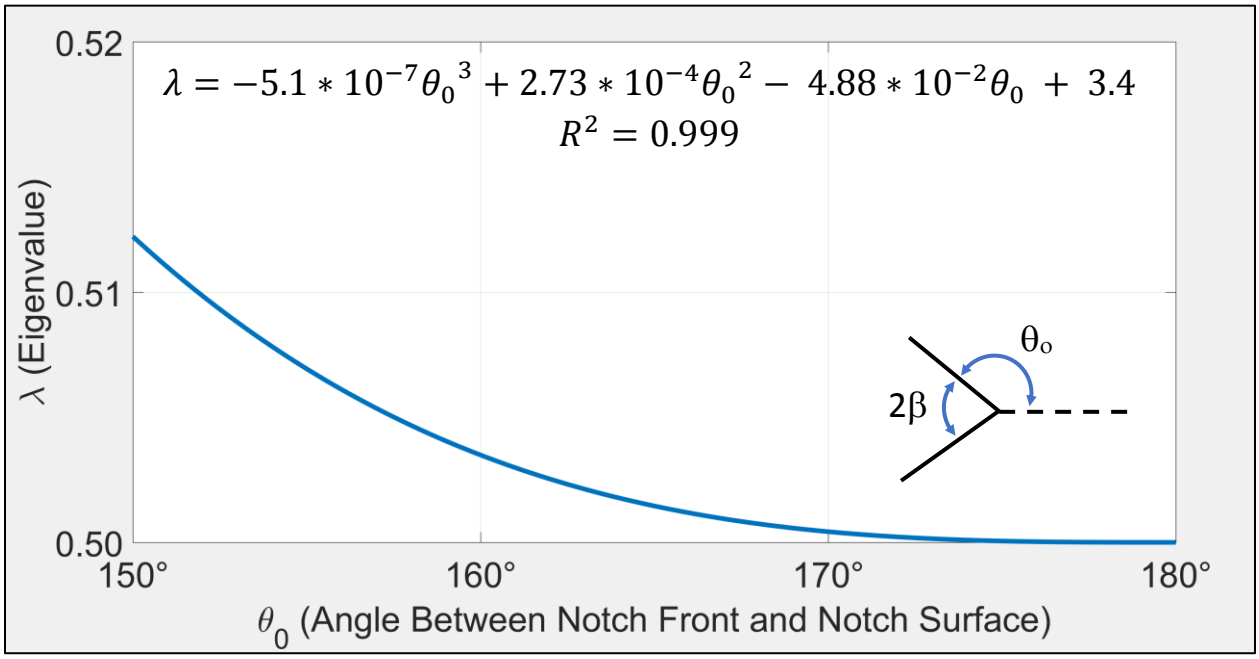

Figure 4- 10: Practical solution range of characteristic function for FDM Parts

Using third order polynomial the curve in figure 4-10 was fitted, as shown in figure 4-11.

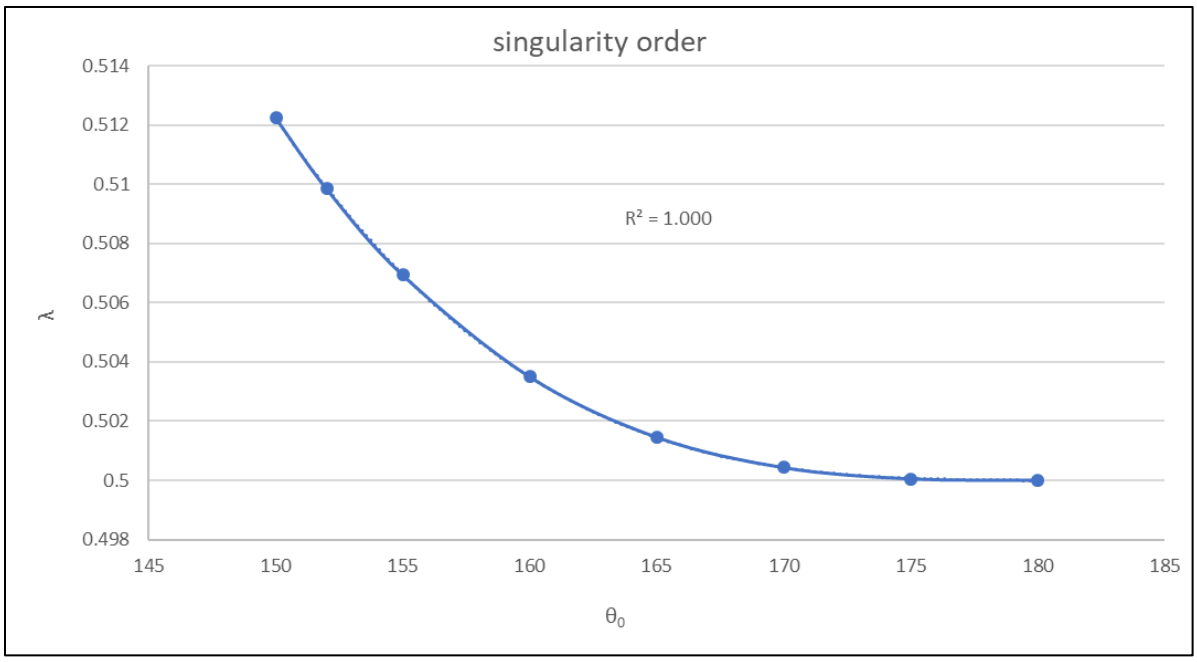

Figure 4- 11: Third Order Polynomial Curve Fitting for 150o< θ0<180º

Singularity orders for different values of 150 < θ0 <180 can be found from:

$$\lambda = -5.09 * 10^{-7}{\theta_0}^3 + 2.73 * 10^{-4}{\theta_0}^2 - 4.87 * 10^{-2}\theta_0 + 3.41 \quad (4.49)$$

From Figures 4-9, 4-10 and 4-11 it is concluded that the singularity order of FDM notches do not significantly change since the notch angles stay in the 0.5 singularity order range. Therefore, notches exist in FDM parts can be assumed to be hairline cracks.

4.4 J-Integral Method:

J-Integral method for stress intensity calculations is the most preferred and accurate method[34, 35]. J-integral method gives accurate results and it is convenient to utilize (4.50)

for a wide range of LEFM problems[36, 37]. G. B. Sinclair and colleagues showed in their research that J – Integral solution for sharp notches in elastic materials, provides accurate estimates of stress intensity Factor[37]. For J-integral method high element orders are not required and element size of 1/10 of the crack length gives accurate SIF result.[34].

$$J = \int_{\Gamma} W\,dy - \boldsymbol{T_i}\,\frac{d\boldsymbol{u_i}}{dx}\,ds = \int_{\Gamma} (W\,n_x - \boldsymbol{T_i}\,\frac{d\boldsymbol{u_i}}{dx})\,ds$$

Γ is defined as a continuous and differentiable curve starting from one crack surface to another crack surface. This integration is evaluated in counterclockwise direction. The crack tip is located inside the curve.

W is strain energy density:

$$W = 0.5\,(\sigma_x\varepsilon_x + \sigma_y\varepsilon_y + 2\sigma_{xy}\varepsilon_{xy)} \tag{4.51}$$

T is traction vector defined in outward normal direction of Γ:

$$T = (\sigma_x.n_x + \sigma_{xy}.n_y, \sigma_y.n_y + \sigma_{xy}.n_x) \tag{4.52}$$

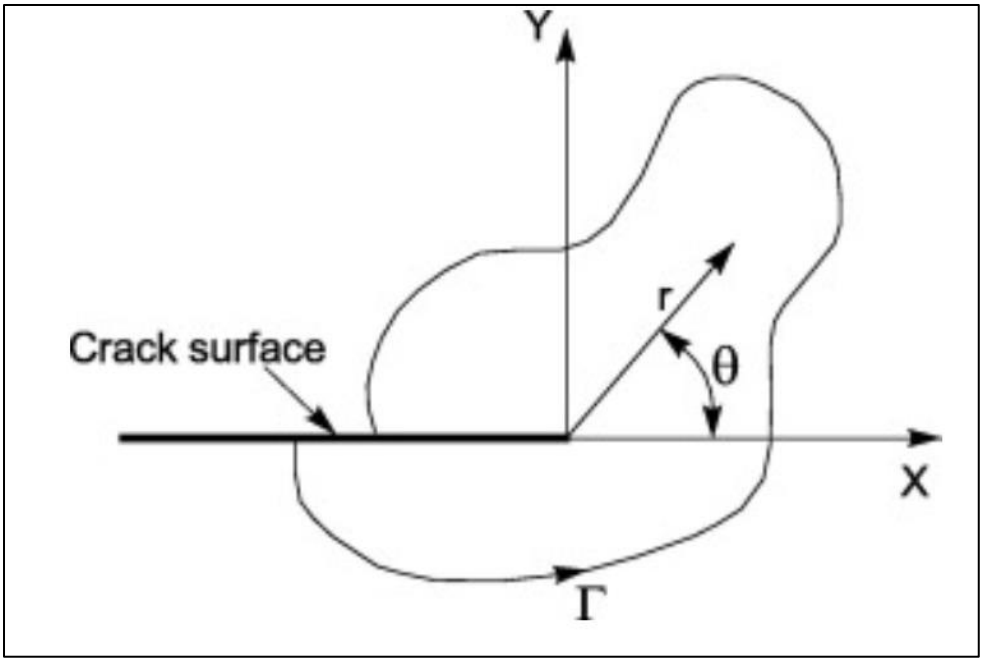

Figure 4- 12: Crack tip and counter clockwise contour for J Integral Calculations

J- Integral characterizes crack tip deformation field in non-linear elastic materials. The power law relationship between plastic strain and stress proposed by Hutchinson[36], Rice and Rosengren[38] is:

$$\frac{\varepsilon}{\varepsilon_0} = \frac{\sigma}{\sigma_0} + \alpha \left(\frac{\sigma}{\sigma_0}\right)^n \tag{4.53}$$

$$\varepsilon_0 = \frac{\sigma_0}{E} \tag{4.54}$$

σ_0 represents the yield stress of the material, α is a dimensionless constant and n is a hardening component.

At areas, very close to the crack tip stress and strain are expressed as:

$$\sigma_{ij} = f(\theta)\left(\frac{J}{r}\right)^{\frac{1}{n+1}} \tag{4.55}$$

$$\varepsilon_{ij} = g(\theta)\left(\frac{J}{r}\right)^{\frac{n}{n+1}} \tag{4.56}$$

For linear elastic materials, n is equal to unity; Therefore, the above equations result in $\frac{1}{\sqrt{r}}$ singularity.

J-integral for linear elastic materials represents the energy release rate. Relationship between energy release rate and stress intensity factor for plane strain models is:

$$\boldsymbol{J = \frac{K^2}{E'}} \tag{4.57}$$

$$\boldsymbol{E' = \frac{E}{1-\nu}} \tag{4.58}$$

Rice [39] proved that J integral has a path independent property as shown below:

$$J = \int_{\Gamma} W\,dy - \boldsymbol{T_i}\,\frac{d\boldsymbol{u_i}}{dx}\,ds = \int_{\Gamma} \left(\frac{\partial W}{\partial x} - \frac{\partial}{\partial x_j}\left(\sigma_{ij}\frac{\partial u_i}{\partial x}\right)\right) dxdy \tag{4.59}$$

$$\frac{\partial \mathrm{W}}{\partial \mathrm{x}} = \frac{\partial \mathrm{W}}{\partial \varepsilon_{\mathrm{ij}}}\frac{\partial \varepsilon_{\mathrm{ij}}}{\partial \mathrm{W}} = \sigma_{\mathrm{ij}}\frac{\partial \varepsilon_{\mathrm{ij}}}{\partial \mathrm{x}} \tag{4.60}$$

$$\varepsilon_{\mathrm{ij}} = 0.5\left(\frac{\partial \mathrm{u_i}}{\partial \mathrm{x_j}} + \frac{\partial \mathrm{u_j}}{\partial \mathrm{x_i}}\right) \tag{4.61}$$

$$\frac{\partial W}{\partial x} = 0.5\ \sigma_{ij}\left[\frac{\partial}{\partial x}\left(\frac{\partial u_i}{\partial x_j}\right) + \frac{\partial}{\partial x}\left(\frac{\partial u_j}{\partial x_i}\right)\right] \tag{4.62}$$

$$\frac{\partial W}{\partial x} = 0.5\ \sigma_{ij}\left[\frac{\partial}{\partial x_j}\left(\frac{\partial u_i}{\partial x}\right) + \frac{\partial}{\partial x_i}\left(\frac{\partial u_j}{\partial x}\right)\right] \tag{4.63}$$

$$\frac{\partial W}{\partial x} = \sigma_{ij}\frac{\partial}{\partial x_j}\left(\frac{\partial u_i}{\partial x}\right) \tag{4.64}$$

By adding and subtracting

$$\frac{\partial \sigma_{ij}}{\partial x_j}\left(\frac{\partial u_i}{\partial x}\right) \tag{4.65}$$

We get

$$\frac{\partial W}{\partial x} = \frac{\partial}{\partial x_j}\left(\sigma_{ij}\frac{\partial u_i}{\partial x}\right) - \frac{\partial \sigma_{ij}}{\partial x_j}\frac{\partial u_i}{\partial x} \tag{4.66}$$

Now from Eq 4.59 and Eq 4.66

$$J = \int_{\Gamma} W\,dy - T_i\,\frac{du_i}{dx}\,ds = -\int_{A}\left(\frac{\partial \sigma_{ij}}{\partial x_j}\frac{\partial u_i}{\partial x}\right) dx dy \tag{4.67}$$

If and only if $A_j = \int_A \left(\frac{\partial \sigma_{ik}}{\partial x_k}\frac{\partial u_i}{\partial x}\right) dx dy = 0$ then left-hand side of the above Eq becomes zero. Therefore Rice [39] concluded that J- integral is path independent.

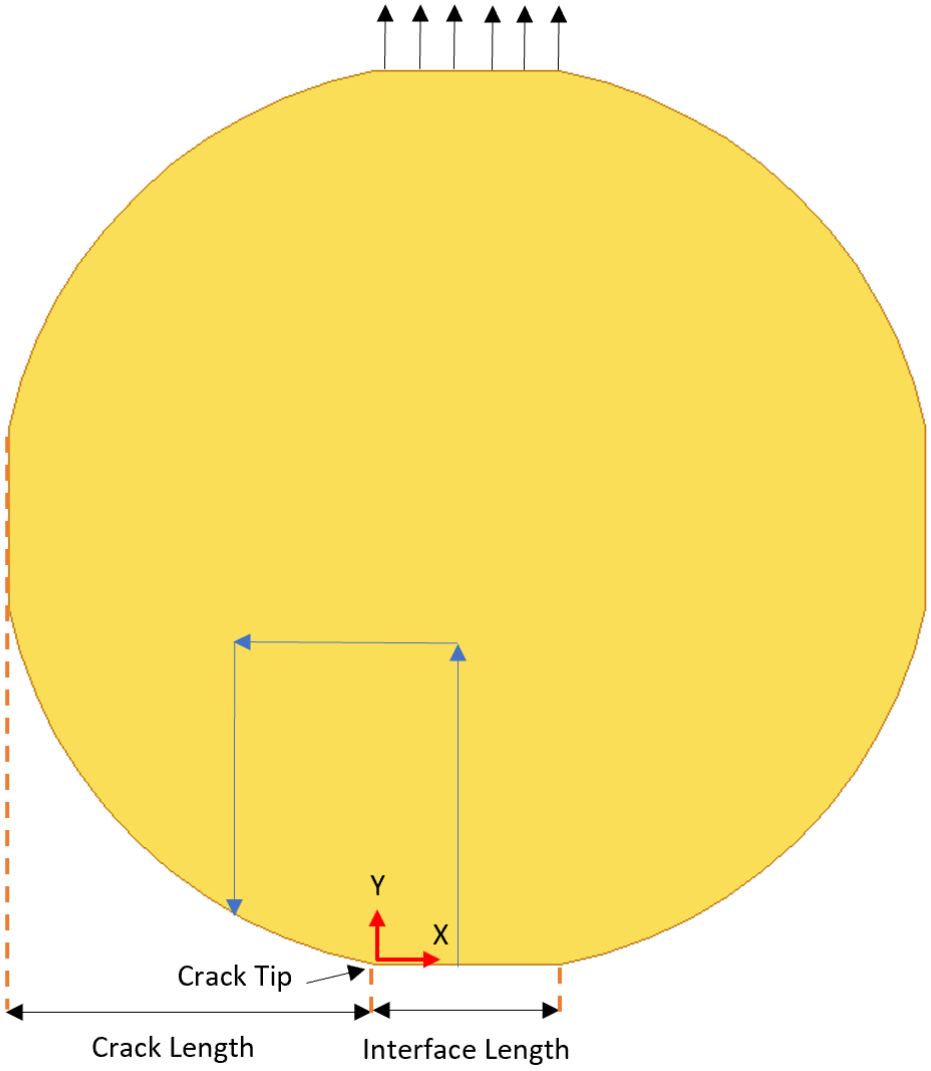

Figure 4- 13: J-Integral FEM Set Up

$$L_{interface} = 2.r.\cos\left(\frac{\pi}{2} - \cos^{-1}\left(\frac{r - r.gp}{r}\right)\right) \quad (4.68)$$

$$a_{crack} = \frac{d_f - L_{interface}}{2} \quad (4.69)$$

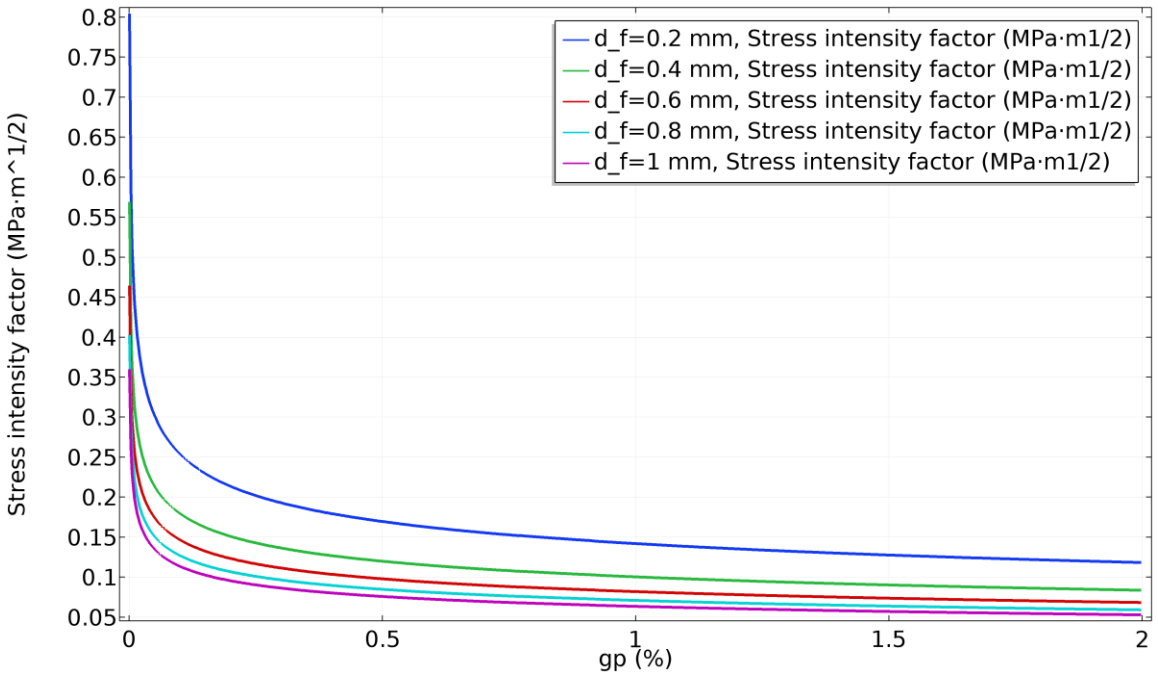

Figure 4- 14: Change in SIF for Different Airgap Settings

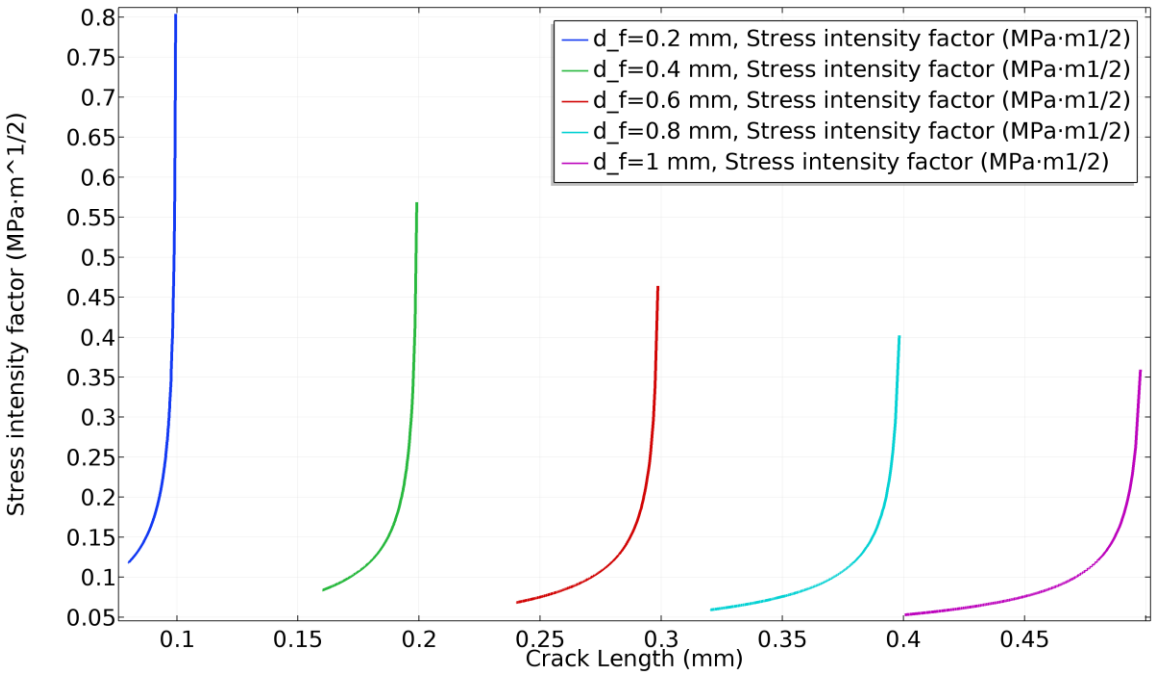

Figure 4- 15: Change in SIF for Different Filament Diameter and Crack Length

4.5 Conclusion:

In this chapter, two methods were used to study the stress intensity factor for singularity points at the interface between filaments. J-integral and eigenvalue expansion method both provided expectable results. However, as the negative gap increases between filaments the error in J-integral values increases as the angle of the notch at the interface becomes wider. A third order polynomial equation was proposed for singularity order determination of FDM parts with negative gap settings less than 3%.

The results of this study also prove that higher negative gap setting and larger notch angle at the interface between filaments result in significant improvements in fracture properties of the FDM part.

Chapter 5:

Summary, Recommendations, and Future Directions

5.1 Summary:

A comprehensive study of different physics involved in FDM process was performed in this research.

Results of the non-isothermal sintering process indicate that the effects of polymer sintering in the final interface between filaments is not as important as the effect of negative gap setting. As higher negative gap settings results in longer interface between the filaments than the polymer sintering process. It was also shown that the interface length increase due to polymer sintering process is greatly dependent on the parameter used in FDM process, such as filaments diameter and print speed.

The diffusion models showed the importance of initial diffusion temperature and the length of the time the temperature at the interface stays above glass transition temperature in the final development of mechanical properties between filaments. The results suggest that mechanical properties of the FDM parts may be increased by utilizing heat treatment process. It was also shown that the higher negative gap setting does not directly affect the intermolecular diffusion rate at the interface; however, due to the fact that more molecules experience the highest initial diffusion temperature stronger mechanical properties are achieved with higher negative gap settings.

A detailed study of the singularity point in the FDM parts was conducted in chapter 4. The results suggest that with negative gap settings of 2~3 % stress singularity order stays close to the stress singularity order of hairline crack and classical fracture mechanics methods could be applied to the FDM parts. It was also shown that the stress intensity factor of the singularity point could be greatly reduced by increasing the negative gap settings or changing the cross-section geometry of the filaments and the extrusion nozzle.

5.2 Conclusion:

The results presented in this research prove that the interfacial properties of FDM parts can be significantly improved by:

1. Using the highest extrusion temperature
2. Using higher speed
3. Increasing filament's diameter
4. Increasing negative gap setting
5. Heat treatment of finished FDM parts results in increase of molecular diffusion, hence higher interfacial properties are achieved.

It was shown that in all print strategies higher negative gap setting provides more interfacial mechanical improvements than polymer sintering effect. Therefore, new extrusion geometries could be utilized to optimize the interface length of the filaments. Figure 4-16 shows a possible optimized geometry for filaments and extrusion nozzle.

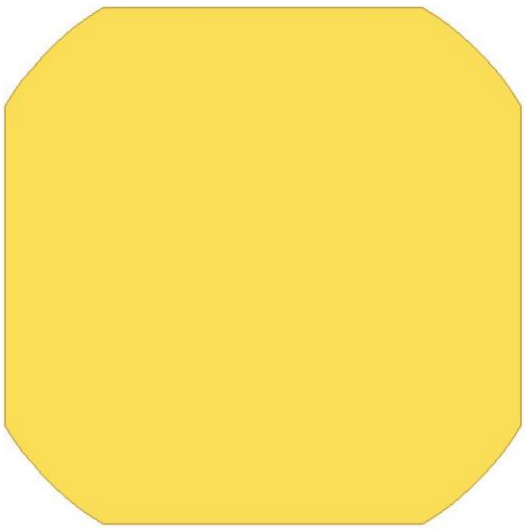

Figure 5-1: A Possible Cross-Section for Improved Interfacial Properties

The cross section suggested in Figure 4-16, provides the following improvements:

1. Void density of the FDM parts could be reduced which results in higher mechanical and thermal properties.
2. Maximum wetting length could be achieved for sintering process
3. Maximum sintering initiation temperature could be achieved, by increasing the thermal capacity of the cross section
4. Maximize the interface area that experience the high initial diffusion temperature.
5. Minimize the notch angle between filaments, which results in minimizing the notch stress intensity factor by increasing the singularity order of the notch.

5.3 Future Directions:

Future research should be focused on:

1. Development of Arrhenius equations for different materials used in FDM process.
2. Extrusion Nozzle cross-section optimization to maximize the interface length between the filaments. (with proposed cross-section geometry shown in Figure 5-1)
3. Study of the effect of thermal expansion of the polymers on the interface length of the filaments.
4. Heat treatment process for FDM parts.
5. Ways to increase thermal capacity of the polymers
6. Ways to improve molecular diffusion at the interface using different techniques (e.g.. local heating using Microwave)

References:

1. Asgarpour, M., et al., *Characterization and modeling of sintering of polymer particles.* Journal of Applied Polymer Science, 2011. **119**(5): p. 2784-2792.
2. Li, L., et al., *Investigation of Bond Formation in FDM Process*. 2004.
3. Rodriguez Matas, J.F., *Modeling the mechanical behavior of fused deposition acrylonitrile-butadiene-styrene polymer components*. 1999, University of Notre Dame: Ann Arbor. p. 198.
4. Sun, Q., et al., *Effect of processing conditions on the bonding quality of FDM polymer filaments.* Rapid Prototyping Journal, 2008. **14**(2): p. 72-80.
5. Pokluda, O., C.T. Bellehumeur, and J. Vlachopoulos, *Modification of Frenkel's model for sintering.* American Institute of Chemical Engineers. AIChE Journal, 1997. **43**(12): p. 3253.
6. Bellehumeur, C., et al., *Modeling of Bond Formation Between Polymer Filaments in the Fused Deposition Modeling Process.* Journal of Manufacturing Processes, 2004. **6**(2): p. 170-178.
7. Lontz, J.F., *Sintering of Polymer Materials*, in *Sintering and Plastic Deformation: Proceedings of the First Symposium on Fundamental Phenomena in the Material Sciences*, L.J. Bonis and H.H. Hausner, Editors. 1964, Springer US: Boston, MA. p. 25-47.
8. Hull, C.W., *Apparatus for production of three-dimensional objects by stereolithography*. 1986, Google Patents.

9. Syed, H.M., *Intelligent rapid prototyping with fused deposition modelling.* Rapid Prototyping Journal, 1996. **2**(1): p. 24-33.

10. Cooke, M.N., et al., *Use of stereolithography to manufacture critical-sized 3D biodegradable scaffolds for bone ingrowth.* Journal of Biomedical Materials Research Part B: Applied Biomaterials, 2003. **64B**(2): p. 65-69.

11. Cooperstein, I., M. Layani, and S. Magdassi, *3D printing of porous structures by UV-curable O/W emulsion for fabrication of conductive objects.* Journal of Materials Chemistry C, 2015. **3**(9): p. 2040-2044.

12. Tumbleston, J.R., et al., *Continuous liquid interface production of 3D objects.* Science (New York, N.Y.). **347**(6228): p. 1349-1352.

13. Li, L., *Analysis and fabrication of FDM prototypes with locally controlled properties*. 2002, University of Calgary (Canada): Ann Arbor. p. 175.

14. Li, L., et al., *Composite modeling and analysis for fabrication of FDM prototypes with locally controlled properties.* Journal of Manufacturing Processes, 2002. **4**(2): p. 129-141.

15. Sun, Q., *Bond formation between polymer filaments in fused deposition modeling process*, in *Chemical and Petroleum Engineering, University of Calgary*. 2005, University of Calgary: http://hdl.handle.net/1880/42034.

16. F., R.J., T.J. P., and R.J. E., *Mechanical behavior of acrylonitrile butadiene styrene fused deposition materials modeling.* Rapid Prototyping Journal, 2003. **9**(4): p. 219-230.

17. Wool, R.P. and K.M. O'Connor, *A theory crack healing in polymers.* Journal of Applied Physics, 1981. **52**(10): p. 5953-5963.

18. Bergman, T.L., et al., *Fundamentals of Heat and Mass Transfer*. Vol. 997. 2011.

19. Scardovelli, R.Z., Stephane, *Direct numerical simulation of free-surface and interfacial flow.* Annual Review of Fluid Mechanics; Palo Alto, 1999. **31**: p. 567.

20. Gerbeau, J.F. and T. Lelièvre, *Generalized Navier boundary condition and geometric conservation law for surface tension.* Computer Methods in Applied Mechanics and Engineering, 2009. **198**(5): p. 644-656.

21. Multiphysics, C., *Comsol Multiphysics User's Guide*. 2018, ,Stockholm, Sweden: COMSOL AB.

22. Multiphysics, C., *COMSOL Multiphysics Documentation.* p. www.comsol.com.

23. Rankouhi, B., et al., *Failure Analysis and Mechanical Characterization of 3D Printed ABS With Respect to Layer Thickness and Orientation.* Journal of Failure Analysis and Prevention, 2016. **16**(3): p. 467-481.

24. Anna, B. and G. Selçuk, *Mechanical characterization of parts fabricated using fused deposition modeling.* Rapid Prototyping Journal, 2003. **9**(4): p. 252-264.

25. Prager, S. and M. Tirrell, *The healing process at polymer–polymer interfaces.* The Journal of Chemical Physics, 1981. **75**(10): p. 5194-5198.

26. Gennes, P.G.d., *Reptation of a Polymer Chain in the Presence of Fixed Obstacles.* The Journal of Chemical Physics, 1971. **55**(2): p. 572-579.

27. Yang, F. and R. Pitchumani, *Healing of Thermoplastic Polymers at an Interface under Nonisothermal Conditions.* Macromolecules, 2002. **35**(8): p. 3213-3224.

28. Bastien, L.J. and J.W. Gillespie, *A non-isothermal healing model for strength and toughness of fusion bonded joints of amorphous thermoplastics.* Polymer Engineering & Science, 1991. **31**(24): p. 1720-1730.

29. Wu, S., *Polymer Interface and Adhesion.* Marcel Dekker,New York, 1982.

30. Lee, W.I. and G.S. Springer, *A Model of the Manufacturing Process of Thermoplastic Matrix Composites.* Journal of Composite Materials, 1987. **21**(11): p. 1017-1055.

31. Anderson, T.L. and T.L. Anderson, *Fracture Mechanics: Fundamentals and Applications, Third Edition*. 2005: Taylor & Francis.

32. M.L.Williams, *Stress Distribution at the Base of a Stationary Crack.* Journal of Applied Mechanics, 1956. **24** p. 109-114.

33. Williams, M.L., *Stress Singularities Resulting From Various Boundary Conditions in Angular Corners of Plates in Extension.* Journal of Applied Mechanics, 1952. **19**: p. 526-528.

34. Han, Q., et al., *Determination of stress intensity factor for mode I fatigue crack based on finite element analysis.* Engineering Fracture Mechanics, 2015. **138**: p. 118-126.

35. J. Thomas, K.C.K., J. S. Crompton *Small Scale Yielding Model for Fracture Mechanics*, in *2014 COMSOL Conference*. 2014, Comsol Multiphysics.

36. Hutchinson, J.W., *Singular behaviour at the end of a tensile crack in a hardening material.* Journal of the Mechanics and Physics of Solids, 1968. **16**(1): p. 13-31.

37. Sinclair, G.B., M. Okajima, and J.H. Griffin, *Path independent integrals for computing stress intensity factors at sharp notches in elastic plates.* International Journal for Numerical Methods in Engineering, 1984. **20**(6): p. 999-1008.

38. Rice, J.R. and G.F. Rosengren, *Plane strain deformation near a crack tip in a power-law hardening material.* Journal of the Mechanics and Physics of Solids, 1968. **16**(1): p. 1-12.

39. Rice, J.R., *A PATH INDEPENDENT INTEGRAL AND THE APPROXIMATE ANALYSIS OF STRAIN CONCENTRATION BY NOTCHES AND CRACKS.* BROWN UNIV PROVIDENCE RI DIV OF ENGINEERING, May 1967.

40. Q. Sun, G.M.R., C.T. Bellehumeur and P.Gu, *Experimental Study of the Cooling Characteristics of Polymer Filaments in FDM and Impact on the Mesostructures and Properties of Prototypes.*, in *Solid Freeform Fabrication Symposium*. 2003: Austin, TX,. p. 313-323.